



**Politecnico  
di Torino**

**Politecnico di Torino**

Corso di Laurea Magistrale in Ingegneria Civile  
Anno Accademico 2023/2024  
Sessione di Laurea Ottobre 2023

# **Monitoraggio della Salute Strutturale delle Infrastrutture Civili Attraverso Tecniche Innovative**

Sviluppo di un Approccio Automatico all'analisi Modale Operativa

Relatori:

Prof. Gian Paolo Cimellaro  
Dr. Alessandro Cardoni

Candidato:

Amir Reza Elahi





**Politecnico  
di Torino**

**Politecnico di Torino**

Master of Science in Civil Engineering  
Academic Year 2023/2024  
Graduation Session October 2023

# **Structural Health Monitoring of Civil Infrastructures Using Innovative Techniques**

Development of An Automated Operational Modal Analysis  
Approach

Supervisors:

Prof. Gian Paolo Cimellaro  
Dr. Alessandro Cardoni

Candidate:

Amir Reza Elahi



STRUCTURAL HEALTH MONITORING OF CIVIL INFRASTRUCTURES USING  
INNOVATIVE TECHNIQUES

A Thesis

By

AMIR REZA ELAHI

Submitted to the Department of Structural, Geotechnical and Building Engineering of

POLITECNICO DI TORINO

in partial fulfillment of the requirements for the degree of

MASTER OF SCIENCE

Chair of committee, Chair name

Committee members: Committee member 1

Committee member 2

Committee member 3

Head of Department, Head of Department

October 2023

Major Subject: Structures and Infrastructures

Copyright 2023 Amir Reza Elahi



## ABSTRACT

Infrastructures play a pivotal role in community development, exerting an immense influence on economic growth. Structural Health Monitoring (SHM) is a multidisciplinary field encompassing the infrastructure's monitoring and condition assessment. Within this field, Operational Modal Analysis (OMA) offers a wide range of vibration-based monitoring solutions to address concerns regarding the integrity of civil assets while ensuring uninterrupted serviceability. OMA employs procedures to extract damage-sensitive features, indicating the structural integrity, without any need to measure the input excitation. This thesis focuses on adapting Automated Frequency Domain Decomposition (AFDD) using the Modal Assurance Criterion (MAC) to acquire essential modal properties such as natural frequencies and mode shapes.

In the first part, after formulating the adapted methodology, the optimal performance of AFDD is established through a comprehensive sensitivity analysis using a Machine Learning (ML) algorithm. The analysis considers various factors influencing the extracted modal properties to develop a robust procedure. These influential factors include noise levels, spatial resolution of sensors, recordings duration, and variation of hyperparameters present in the methodology. In this regard, field measurements from a cable-stayed bridge are analyzed by AFDD, optimizing the method by constructing stabilization diagrams. In these diagrams, the extracted natural frequencies from AFDD are compared with the data corresponding to the Finite Element (FE) counterparts. Gaussian Mixture Model (GMM) is employed to cluster the extracted frequencies based on their accuracy and determine the optimal ranges for each hyperparameter of the AFDD.

Furthermore, this thesis presents an extensive output-only modal identification of various infrastructures using three distinct case studies: the Yonghe cable-stayed bridge, PolyU footbridge,

and Moletta tower in the Maximus archaeological site. The dynamic characterization is performed by traditional Frequency Domain Decomposition (FDD), optimized AFDD, and covariance-driven Stochastic Subspace Identification (cov-SSI). The accuracy of the optimized AFDD method is evaluated, along with the potential limitations of each approach. Specifically, the effectiveness of these methods in identifying closely spaced, weakly excited modes, dealing with spurious peaks, and accurately identifying complex ones is examined. The study reveals valuable insights for each case study and highlights the risks of failing to identify particular vibrational modes when implementing OMA procedures.

In summary, this thesis presents an optimized AFDD approach for the long-term extraction of modal properties while comparing its performance with other well-defined methods. The findings from the case studies shed light on the strengths and limitations of each applied approach, offering valuable insights for the health assessment and monitoring of civil infrastructures.

Keywords: Modal identification, Automated Frequency Domain Decomposition, Gaussian Mixture Model, Covariance- driven stochastic subspace identification, Cable-stayed bridges, Footbridges, Archeological sites.

## **DEDICATION**

In the name of God, the Compassionate, the Merciful, with thanks to God and greetings to his chosen servants.

Dedicated to:

The divinely knowledgeable master, the great scholar, Haaj Zainolabedin Khan Ebrahimi (may God protect him)

## ACKNOWLEDGMENT

I would like to express my heartfelt gratitude to all those who have supported and guided me throughout the course of my research and the completion of this thesis.

First and foremost, I am deeply thankful to my thesis advisor, Professor Gian Paolo Cimellaro, for their unwavering support, invaluable guidance, and endless patience. Their expertise and mentorship were instrumental in shaping the direction of this work and improving the quality of my research.

I also appreciate Dr. Alessandro Cardoni for constructive feedback, stimulating discussions, and the knowledge he shared during my academic journey. I am indebted to Dr. Marco Domaneschi for their valuable suggestions too.

Furthermore, I am sincerely grateful to my family for their unconditional love and encouragement, which provided the emotional sustenance necessary to navigate through the challenges of this endeavor. Their persistent faith in me was an immense source of motivation.

I appreciate all my friends and colleagues, Mohammad, Mahdi, Hamed, Raffaele, and Andrea. Their diverse perspectives and encouragement have been instrumental in refining my ideas.

Lastly, I would like to acknowledge Politecnico di Torino, which made this research possible.

Amir Reza Elahi



## NOMENCLATURE

SHM	Structural Health Monitoring
EMA	Experimental Modal Analysis
OMA	Operational Modal Analysis
FE	Finite Element
RDT	Random Decrement Technique
ERA	Eigensystem Realization Algorithm
SSI	Stochastic Subspace Identification
Data-SSI	Data-driven Stochastic Subspace Identification
Cov-SSI	Covariance-driven Stochastic Subspace Identification
GMM	Gaussian Mixture Model
MLE	Maximum Likelihood Estimation
PDFs	Probability Density Functions
EM	Expectation-Maximization
SVD	Singular Value Decomposition
SOBI	Second Order Blind Identification
FDD	Frequency Domain Decomposition
PSD	Power Spectral Density
DFT	Discrete Fourier Transform
EFDD	Enhanced Frequency Domain Decomposition
AOMA	Automated Operational Modal Analysis
ML	Machine Learning
CNN	Convolutional Neural Network

MDOF	Multi Degree of Freedom
MAC	Modal Assurance Criterion
EVD	Eigen Value Decomposition
CF	Correlation Function
SDOF	Single Degree of Freedom
FRF	Frequency Response Function

## TABLE OF CONTENTS

Abstract.....	i
Dedication.....	iii
Acknowledgment.....	iv
Nomenclature.....	vi
Table of Contents.....	viii
List of Figures.....	x
List of Tables.....	xiii
1. Introduction.....	1
1.1. Structural health monitoring of civil infrastructures.....	1
1.2. Operational modal analysis:.....	4
1.3. Automated OMA techniques.....	7
1.4. Objectives and outlines of project.....	10
2. Methodology.....	12
2.1. Gaussian Mixture Model.....	12
2.2. Covariance-driven Stochastic Subspace Identification.....	13
2.3. Traditional Frequency Domain Decomposition.....	16
2.4. Automated Frequency Domain Decomposition.....	19
3. Optimization of Automated Frequency Domain Decomposition.....	22

3.2.	Preprocessing of input.....	24
3.3.	Sensitivity analysis.....	25
4.	Methodology validation.....	40
4.1.	Case study 1: Yonghe cable stayed bridge.....	40
4.2.	Case study 2: PolyU footbridge.....	49
4.3.	Case study 3: Moletta tower in Circo Massimo.....	59
5.	Development of software interface.....	66
6.	Concluding remarks.....	68
7.	References.....	70

## LIST OF FIGURES

Fig. 1-1. Diverse adaptivity of SHM for various infrastructures. ....	2
Fig. 1-2. Triton accelerogram used in SHM tasks at Politecnico di Torino. ....	3
Fig. 2-1. The flowchart of the AFDD algorithm. ....	21
Fig. 3-1. The Yonghe cable stayed bridge in China. ....	22
Fig. 3-2. The SHM configuration proposed for the Yonghe cable-stayed bridge. ....	23
Fig. 3-3. FE model of the Yonghe cable-stayed. ....	23
Fig. 3-4. The effect of $\alpha$ variation on the AFDD's outcomes. ....	28
Fig. 3-5. The effect of $\alpha$ variation with the noise level: (a) SVD denoising parameter $l=0.05$ , (b) $l=0.20$ , (c) $l=0.35$ , (d) $l=0.50$ , (e) $l=0.75$ . ....	30
Fig. 3-6. The effect of $\alpha$ variation and signal length: Input duration of (a) 5 minutes, (b) 1 hour, (c) 4 hours, (d) 12 hours, (e) 24 hours. ....	32
Fig. 3-7. The effect of $\alpha$ variation with the number of sensors, and their configuration: (a) original layout, (b) layout 1, (c) layout 2, (d) layout 3, (e) layout 4, (f) sensors layout. ....	34
Fig. 3-8. The effect of MAC variation with sampling frequency on the AFDD outcomes: Sampling frequencies of (a) $F_s=100$ Hz, (a) $F_s=100$ Hz, (b) $F_s=20$ Hz, (c) $F_s=150$ Hz, (d) $F_s=300$ Hz, (e) $F_s=400$ Hz. ....	36
Fig. 3-9. The effect of MAC variation and number of required peaks on the AFDD outcomes: (a) No. peak is 3, (b) No. peak is 5, (c) No. peak is 7, (d) No. peak is 9. ....	37
Fig. 3-10. Qualitative correct estimation for each $\alpha$ value. ....	38
Fig. 3-11. The sub-optimal/optimal ranges derived from sensitivity analysis for each case. ....	39
Fig. 4-1. The acceleration recorded by sensor 14 on the cable stayed bridge. ....	40

Fig. 4-2. AFDD analysis of the cable-stayed bridge for 1-hour signal: (a) selected peaks in the SV spectrum, and (b) MAC evaluation for the first selected peak and modal domain assessment....	41
Fig. 4-3. 3D deformed configuration of the Yonghe cable-stayed bridge.....	42
Fig. 4-4. Stabilization diagram for the cov-SSI analysis of the Yonghe cable-stayed bridge for 1-hour record. ....	42
Fig. 4-5. AFDD analysis of the cable-stayed bridge for 12-hour signal .....	43
Fig. 4-6. Stabilization diagram for the cov-SSI analysis of the Yonghe cable-stayed bridge for 12-hour record. ....	44
Fig. 4-7. Comparison of derived mode shapes for Yonghe cable-stayed bridges (1 h duration), (a) first mode, (b) second mode, (c) third mode, (d) 4 <sup>th</sup> mode, (e) 5 <sup>th</sup> mode, (f) 6 <sup>th</sup> mode.....	47
Fig. 4-8. Comparison of derived mode shapes for Yonghe cable-stayed bridges (12 h duration), (a) first mode, (b) second mode, (c) third mode, (d) 4 <sup>th</sup> mode, (e) 5 <sup>th</sup> mode, (f) 6 <sup>th</sup> mode.....	49
Fig. 4-9. PolyU footbridge located in the Hong Kong Polytechnic University. ....	50
Fig. 4-10. The SHM layout mounted on the PolyU footbridge. ....	51
Fig. 4-11. Vertical acceleration recorded by sensor B2 on the PolyU footbridge. ....	51
Fig. 4-12. The automatically selected peaks in the SV spectrum by AFDD analysis for PolyU..	52
Fig. 4-13. 3D deformed configuration of the PolyU footbridge. ....	53
Fig. 4-14. The resultant stabilization diagram for the PolyU footbridge.....	54
Fig. 4-15. Comparison of extracted mode shapes from PolyU footbridge, (a) first mode, (b) second mode, (c) third mode, (d) fourth mode. ....	57
Fig. 4-16. (a) The general view of Maximus circus, (b) Moletta tower, (c) spiral stair case.....	59
Fig. 4-17. (a) Moletta tower (b) side view of tower. (c) section C-C. (d) section A-A. ....	59
Fig. 4-18. Sensor placement on the Moletta tower. ....	60

Fig. 4-19. SV spectra and automatically selected frequencies by the AFDD algorithm in (a) x-direction and (b) y-direction. ....	61
Fig. 4-20. Mode shapes of the Moletta Tower. ....	63
Fig. 4-21. Obtained stabilization diagrams for Moletta tower. (a) x-direction, (b) y-direction....	64
Fig. 5-1. A view of the developed software. ....	67

## LIST OF TABLES

Table 1. Comparison of the Yonghe cable-stayed bridge frequencies. ....	45
Table 2. Comparison of the Poly-U footbridge frequencies. ....	55
Table 3. Comparison of the Moletta Tower frequencies. ....	65

# 1. INTRODUCTION

## 1.1. Structural health monitoring of civil infrastructures

Civil infrastructures constitute a significant part of societies, providing essential means for transportation, commerce, and cultural enrichment. The civil assets, ranging from bridges to buildings, have a pivotal contribution into our daily lives. However, as they degrade and face various harsh environmental conditions, ensuring their integrity and safety becomes a critical concern. Under these circumstances, Structural Health Monitoring (SHM) emerges as a vital field within the civil engineering discipline, providing reliable solution in monitoring of aged assets.

SHM is a multidisciplinary field which encompass the continuous monitoring of an asset's condition and integrity. Generally, its application result in the detection and diagnosis of structural defects in real time, allowing for proper interventions to avoid catastrophic failures. By implementing SHM methodologies, engineers widen the lifespan of infrastructures, lessen the maintenance costs, and improve user safety.

The traditional inspection methods, primarily visual inspections, are periodic and limited in scope. However, the SHM utilization involves a continuous and automatic monitoring scheme. Furthermore, it is able to record subtle changes occurred in the behavior of a structure over time, even those not detected through visual inspection. Early detection of defects such as the formation of cracks, plastic strains and deformations, or material degradation enables engineers to address them on time and avoid their escalation.

SHM is consisted of innovative tools with versatile range of application. It can be applied to a wide range of civil assets, from cable-stayed bridges and under water tunnels to commercial buildings and immense dams. In the monitoring of each asset, unique challenges exist where SHM provides tailored solutions to address them on a proper time. Thus, with a high level of adoption

without any dependence on complexity or scale of the structure, SHM can be utilized to offer effective monitoring.



(a) Sunshine Skyway Cable-stayed bridge, Florida, US.



(b) Torre della Ghirlandina, Modena, Italy.

Fig. 1-1. Diverse adaptivity of SHM for various infrastructures.

At the core of SHM, sophisticated sensor technologies play a vital role. They are optimally instrumented on or embedded into the structure to record a variety of data, including vibrations, strains, and temperature. The collected data is later processed to attain insights into the structural integrity and performance. Advances in the development of sensors have led to the technology with high accuracy and reliable systems.

SHM not only does enhance the user safety but also proven to be a cost-effective solution in the long term. By early detection of defects, the need for extensive and costly retrofits or replacements is subsided. In addition, in the era of growing concerns about the climate changes, it contributes to enhance sustainability.



Fig. 1-2. Triton accelerogram used in SHM tasks at Politecnico di Torino.

In details, by extending the service life of existing infrastructures through optimal retrofiting, it reduce the demand for new constructions that is resource-intensive and environmentally incompatible. The sustainable asset managements, obtained by SHM outcomes, align with global attempts to minimize the environmental impact of infrastructures developments.

Another advantage of this broad discipline is its valuable information for stakeholders obtained from the generated monitoring data. It enables them to make proper decisions about maintenance, and retrofiting strategies. Additionally, this data-driven field can be established to optimize the design of future structures, incorporating lessons learned from the monitoring process.

In the realm of civil engineering, two primary approach of Experimental Modal Analysis (EMA) and Operational Modal Analysis (OMA) exist. EMA involves performing controlled tests on a structure, with known excitation sources like shakers or impact hammers, to extract its modal properties such as natural frequencies, mode shapes, and damping ratios. These properties serve as a foundation to understand a structure's dynamic behavior. OMA, on the other hand, focuses on achieving modal properties from ambient vibrations, making it well-suited for monitoring real-world structures. SHM can employs extracted outputs from EMA to establish baseline

characteristics and subsequently use OMA techniques in continuous monitoring of civil assets. By comparing real-time operational modal parameters to baseline values, irregularities are detected as an indication of damage. However, in majority of SHM tasks, it is highly impossible to prepare proper boundary conditions or sufficient excitation of complex infrastructures. Consequently, the use of contemporary technology such as point cloud measurement incorporated with Finite Element (FE) modelling are replaced with EMA solution.

## 1.2. Operational modal analysis:

Operational Modal Analysis (OMA) is a distinctive field within the SHM that focuses on extracting vital data about the dynamic behavior of structures under operational conditions. It is a rigorous tool for assessing the health and performance of civil assets, without the interruption of serviceability. OMA allows engineers to get details about the modal properties of structures, such as natural frequencies, mode shapes, and damping ratios, under real-world operating conditions. The modal properties are further incorporated into the condition assessments of existing structures (Sunca et al. 2021), updating of FE models (Sabamehr et al. 2018), damage identification (Limongelli and Giordano 2020), and vibrational control policies (Pereira et al. 2022). Additionally, OMA techniques are classified as the primary nondestructive techniques that are compatible with historical sites in the context of monitoring and characterization. In this section, the methodologies employed in OMA are explored, both in the time and frequency domains, to better understand the principles and their applications.

The Random Decrement Technique (RDT) is powerful method proposed in the time domain of OMA (Vesterholm et al. 2020). It is useful when dealing with non-stationary input or random excitation, which is well-suited for real-world tasks. The method begins by processing a specific point in the time-domain output signal, often associated with a local peak. This selected

point, known as the reference point, serves as the starting position for analysis. Next, a series of time increments, typically consisting of equal time intervals, are taken in both the forward and backward directions from the reference point. These increments create a set of data segments, each centered on the reference point. Subsequently, the modal properties are extracted from these individual data segments following a certain mathematical manipulations such as applying Eigensystem Realization Algorithm (ERA) (Hill n.d.). This methodology has some limitation in detecting closely spaced modes, and requires extreme computational efforts for large dataset.

In the time domain, one the most primary techniques is Stochastic Subspace Identification (SSI) (VanOverschee, 1996). It excels at extracting modal parameters from ambient vibration response based on their statistical properties. The methodology is divided into Data-driven SSI (Data-SSI) and Covariance-driven SSI (cov-SSI) depending on the processing roots. In Data-SSI, the focus is on the recorded ambient vibration itself. This method does not rely on any specific assumptions about the system or the input excitation. It typically involves Singular Value Decomposition (SVD) techniques that is applied directly to the measured data. Cov-SSI, on the other hand, leverages the covariance matrix of the recorded signal. It assumes that the input excitation is stationary and has specific statistical properties. By analyzing the covariance matrix, the modal properties are estimated. The application of the SSI methodologies entails the estimation of a parameter named model order, which is challenging in the case of dynamically complex structures. Consequently, an iterative approach is employed, where various model orders are assigned to system, and stabilization diagrams are constructed. Within these stabilization diagrams, a separation is made between physical and spurious poles by setting specific thresholds, as elaborated upon in the methodology section.

One of the main challenges in using the SSI procedure is the ambiguous nature of the stabilization diagram, which complicates the differentiation between physical and non-physical dynamic modes. To tackle this issue, Li introduced a time-discrete state-space model that bridges the Second Order Blind Identification (SOBI) (Pan et al. 2022) and cov-SSI algorithms. This novel model is designed to eliminate the ambiguity typically encountered in stabilization diagrams (Li et al. 2022). This innovative methodology directly identifies the model order using SOBI and subsequently employs cov-SSI, eliminating the need to construct stabilization diagrams. Moreover, it distinguishes between physical and noisy modes by analyzing source signals in both the time and frequency domains. Physical modal responses identified by SOBI exhibit sinusoidal decay in the time domain and manifest as spectral peaks in the frequency domain. This approach has demonstrated promising results in characterizing structures such as the Heritage Court Tower in Vancouver and the Longyangxia Dam in China.

In the frequency domain, the general peak picking technique, Frequency Domain Decomposition (FDD) (Brincker et al. 2001), and the least-squares complex-frequency method (Verboven n.d.) are well-defined procedures. When an infrastructure is excited, higher energy is released close to its natural frequencies. This observation led to one of the widely known methodology that is called general peak picking. The method takes a single-step action to determine the Power Spectral Density (PSD) matrix using the Discrete Fourier Transform (DFT). In the PSD, the peaks represent the frequencies at which the structure vibrates most prominently. The method can effectively capture well-separated modes and those with low damping ratios. However, identifying closely-spaced modes is challenging and limited. Therefore, it is solely used to have a preliminary estimate in the number of modes existing in the system.

FDD is another OMA technique that is easy to implement and provides an intuitive interaction with the user. Emerging from the previous method, the FDD can handle its shortcomings by decomposing the resultant PSD using SVD. The modal properties extracted by FDD are natural frequencies and mode shapes, while its enhanced version (EFDD) has the ability to estimate the damping ratios as well. The mathematical backgrounds of this procedure are presented in the methodology section.

In overall, traditional techniques require the expert intervention for analysis and interpretation. Moreover, applying conventional methods to convert ambient vibration responses into dynamic behavior, in real-time condition, is impossible for long term monitoring of many infrastructures. As a result, there has been a significant focus on automating traditional algorithms and mitigating their inherent constraints.

### 1.3. Automated OMA techniques

Automated OMA (AOMA) methods have emerged as a revolutionary approaches to efficiently extract modal parameters in long term monitoring of civil assets. The existing AOMA procedures in the time domain depend on Machine Learning (ML) algorithms for clustering of the poles within a stabilization diagrams (Zhong et al. 2023), (Boroschek and Bilbao 2019). In a primary study by Magalhaes, the cov-SSI procedure was automated by means of a hierarchical clustering algorithm which analyzed the derived poles in a stabilization diagram (Magalhães et al. 2009). Physical modes were distinguished from spurious ones by identifying clusters with a specific number of data points. This algorithm was utilized in the modal identification of the Infante D. Henrique Bridge in Portugal. Nevertheless, it necessitates the establishment of specific thresholds by an expert beforehand.

In a separate study, Ye introduced a novel approach to create stabilization diagrams by combining the NExT/ERA (James et al. 1995) techniques with hierarchical clustering analysis (Ye et al. 2021). Initially, this method was employed on the input data to identify pre-existing modes for various model orders. Subsequently, the collected data underwent filtration using two specific thresholds, which were associated with the damping ratio and a novel consistency index. This filtration process aimed to determine the physical modes within each model order. Once the modes were filtered, a stabilization diagram was constructed, and hierarchical clustering was utilized to automate the analysis of this diagram and extract modal properties. Additionally, during the clustering process, the Tau test was employed to exclude data with discrete damping ratios, which were considered as outliers. This innovative approach was implemented in the characterization of the Guangzhou TV Tower in China. It is important to note that this procedure still requires expert oversight due to the significant number of parameters that need to be preconfigured.

Despite the extensive efforts in developing automated OMA techniques in the time domain, identifying closely spaced modes, lightly excited modes, and generalization for all structural systems is still an open issue. Specifically, the work conducted by Dederichs has highlighted the limitations in the performance of automated approaches using clustering algorithms (Dederichs and Øiseth 2023). It demonstrated the ability of six prominent techniques to extract modal properties automatically from the Hardanger suspension bridge in Norway. Their performance was evaluated based on the known dynamic modes of the bridge in terms of mode detection rate, false mode detections, and duplicate modal detections. For instance, the detection rate derived for these methodologies was in the range of 39.8-81.2%. Overall, each technique exhibited strengths and weaknesses, and their performance was unpredictable for the benchmark.

Just as in the time domain, there have been multiple attempts to automate conventional procedures in the frequency domain. In a study by Kim, the automatic process involved detecting peak regions in the SV spectrum using a Faster R-CNN convolutional neural network and subsequent post-processing to identify vibration modes (Kim and Sim 2019). The network was trained by generated numerical models related to an MDOF system. It outperformed the automated SSI counterpart (Magalhães et al. 2009) in the modal identification of various case studies, achieving an F1 score of 0.92 with less computational effort. Yet, the main limitation of the neural network lies in the distinction of closely-spaced modes with high damping and points located at the boundaries of the peak regions in the SV spectrum.

In another study by Jeong, a deep learning network was trained and validated for automatic peak picking in the SV spectrum to estimate the tension force of bridge cables (Jeong et al. 2021). The network was able to document the changes in the tension force regardless of prior knowledge about the cable dynamics. The study revealed the robustness of automated methods in the frequency domain, suitable for application in various fields of SHM. The benefit of using ML algorithms is their independence from frequency range selection or fixing predefined thresholds. However, they are highly affected by the training data set and their hyperparameter tuning. Consequently, the use of ML algorithms for automating FDD remains experimental.

The AFDD methodology, based on the geometry of mode shapes, was proposed by Brincker to identify closely spaced modes and reduce the reliance on expert intervention (Brincker et al. 2007). It was based on identifying a domain around an SV peak using a modal domain and coherence function. This approach not only automates the EFDD for damping estimations but also distinguishes non-physical modes of vibration. Magalhães further adopted this technique using the Modal Assurance Criterion (MAC). This technique successfully distinguished between vibrational

and non-physical modes in monitoring the Infante D. Henrique Bridge in Portugal. In that study, the MAC threshold was fixed at 0.4 by the user experience. Moreover, it was recommended to perform a preliminary analysis to establish the appropriate thresholds within the methodology, accounting for various factors influencing modal estimations. While using AFDD with MAC has proven to be effective, several factors can influence its accuracy.

#### 1.4. Objectives and outlines of project

The primary limitation of prior studies on the AFDD lies in the identification of non-complex modes of vibration. Besides, introducing a universal set of thresholds compatible with different infrastructures is necessary to avoid further hyper-parameter tuning. In essence, there is a need to set all thresholds to their optimal values, reducing reliance on expert intervention and preliminary analysis of individual case studies. Consequently, the first objective of this study is to investigate the effect of factors characterizing the SHM system, such as noise level, record length, number of sensors, and their configuration, on the performance of adopted AFDD with MAC. A series of sensitivity analyses were performed using real data from the Yonghe cable-stayed bridge in China as the benchmark and data are processed using ML algorithms. This case study is selected since there is a lack of in-depth studies on damage identification and monitoring of cable-stayed bridges based on experimental data (An et al. 2019). As a result, the optimal MAC threshold, accounting for all influential factors, was determined, hindering the need for further hyper-parameter tuning.

The second goal of this study is to test the performance of the AFDD with the optimal thresholds on significantly different and complex case studies by comparing it to the traditional FDD and the cov-SSI. The first case study is the Yonghe cable-stayed bridge in China, which was used to determine the optimal MAC threshold and a different ambient vibration record is considered. The

second case study is the PolyU footbridge on the Main Campus of the Hong Kong Polytechnic University. Footbridges are typically characterized by their complex dynamics and this condition is pronounced with the irregular shape of this case study. Excessive vibration of the Millennium Bridge in London, Changi Mezzanine in Singapore, Toda Park Bridge in Japan, and the hazardous collapse of the Vltava River bridge in Prague highlight the lack of monitoring and SHM studies on them (Xia et al. 2021).

The third application concerns a monumental part of the Circus Maximus in Rome, Italy, namely the Moletta tower. The Circo Maximus is one of the largest archeological sites in the world, and it is highly exposed to various sources of excitations. In addition, it is buried under alluvial soil due to flooding events which makes its dynamic characterization challenging because of soil-structure interaction (Puzzilli et al. 2021).

## 2. METHODOLOGY

In this section, a brief description of cov-SSI and traditional FDD are presented with a focus on the mathematical concepts. It is followed by the formulation of adapted AFDD with MAC.

### 2.1. Gaussian Mixture Model

The Gaussian Mixture Model (GMM) is a widely used unsupervised ML technique for clustering applications. It models complex data sets into separate clusters by combining multiple normal distributions named Gaussian components. In addition, by modeling the normal behavior of datasets, any data point significantly deviating from the learned distribution can be identified as an anomaly. A Gaussian Mixture Model for data point present in the vector  $\mathbf{x}$  with the dimension of  $D$  is defined by a weighted sum of  $K$  Gaussian components expressed as (Bishop 2009):

$$p(\mathbf{x}) = \sum_{k=1}^K \pi_k \cdot \Omega(\mathbf{x} | \boldsymbol{\mu}_k, \boldsymbol{\Sigma}_k) \quad (2-1)$$

In which  $\Omega$  represents the Gaussian distribution, and each Gaussian component is characterized by its mean ( $\boldsymbol{\mu}_k$ ), covariance matrix ( $\boldsymbol{\Sigma}_k$ ), and mixing coefficient ( $\pi_k$ ). To estimate the parameters of the Gaussian components that best describe the input dataset, the Maximum Likelihood Estimation (MLE) is employed. The likelihood function is defined as the product of the Probability Density Functions (PDFs) of the individual Gaussian components, each weighted by its mixing coefficient. Its logarithmic form for the input matrix of  $\mathbf{X} = \{\mathbf{x}_1, \mathbf{x}_2, \dots, \mathbf{x}_N\}$  is:

$$\ln p(\mathbf{X} | \boldsymbol{\pi}, \boldsymbol{\mu}, \boldsymbol{\Sigma}) = \sum_{n=1}^N \ln \left\{ \sum_{k=1}^K \pi_k \cdot \Omega(\mathbf{x}_n | \boldsymbol{\mu}_k, \boldsymbol{\Sigma}_k) \right\} \quad (2-2)$$

Expectation-Maximization (EM) is a robust algorithm to maximize this likelihood solution, which determines  $\boldsymbol{\mu}_k$ ,  $\boldsymbol{\Sigma}_k$ ,  $\pi_k$  iteratively (Dempster et al. 1977). It consists of two main steps: Expectation and maximization steps denoted as E and M steps.

In the E-step, the posterior probabilities, denoted as  $\gamma(z_{nk})$  is computed, which represent the probability of data point  $x_n$  belonging to Gaussian component  $k$ . These probabilities are calculated by the following relation:

$$\gamma(z_{nk}) = \frac{\pi_k \Omega \mathbf{x}_n | \boldsymbol{\mu}_k, \boldsymbol{\Sigma}_k}{\sum_{j=1}^K \pi_j \Omega \mathbf{x}_n | \boldsymbol{\mu}_j, \boldsymbol{\Sigma}_j} \quad (2-3)$$

In the M-step, the GMM parameters are updated using the posterior probabilities calculated in the E-step as follows:

$$\boldsymbol{\mu}_k^{new} = \frac{1}{N_k} \sum_{n=1}^N \gamma(z_{nk}) \mathbf{x}_n \quad (2-4)$$

$$\boldsymbol{\Sigma}_k^{new} = \frac{1}{N_k} \sum_{n=1}^N \gamma(z_{nk}) (\mathbf{x}_n - \boldsymbol{\mu}_k^{new})(\mathbf{x}_n - \boldsymbol{\mu}_k^{new})^T \quad (2-5)$$

$$\pi_k^{new} = \frac{N_k}{N} \quad (2-6)$$

$$N_k = \sum_{n=1}^N \gamma(z_{nk}) \quad (2-7)$$

Where  $N$  is the total number of data points,  $N_k$  is the sum of posterior probabilities for component  $k$ , and  $z_{nk}$  represents the latent variable, indicating the GMM component assignment for data point  $x_n$ .

## 2.2. Covariance-driven Stochastic Subspace Identification

The SSI technique use a state-space model to reformulate a second-order partial differential equation in terms of two separate first-order state and observation problems. Through the cov-SSI identification, the following discrete-time state space model is proposed, where the input is assumed as a white noise signal:

$$\begin{aligned}\mathbf{x}_{k+1} &= \mathbf{A} \cdot \mathbf{x}_k + \mathbf{w}_k \\ \mathbf{y}_k &= \mathbf{C} \cdot \mathbf{x}_k + \mathbf{v}_k\end{aligned}\quad (2-8)$$

Eq.2-8) describes the model, where  $\mathbf{x}_k$  and  $\mathbf{y}_k$  are the state and recorded output vectors at time instant  $k$ . The discrete state and output matrices are  $\mathbf{A}$  and  $\mathbf{C}$  from which the modal properties are extracted. The vector  $\mathbf{w}_k$  represents the model inaccuracy, while  $\mathbf{v}_k$  describes the sensor measurement bias. The analysis begins by estimating the output covariance ( $\mathbf{R}_i$ ) from the correlation between ambient vibration responses summarized in Eq. (2-9).

$$\mathbf{R}_i = \frac{1}{N-i} \sum_{k=1}^{N-i-1} \mathbf{y}_{k+i} \cdot \mathbf{y}_k^T \quad (2-9)$$

Where  $N$  is the length of the discrete output,  $i$  is the time lag parameter, and  $\mathbf{y}_k^T$  is the output's transpose. The Toeplitz matrix  $\mathbf{T}_{||i}$  is then computed from the output covariance ( $\mathbf{R}_i$ ) as indicated in Eq. (2-10).

$$\mathbf{T}_{||i} = \begin{bmatrix} \mathbf{R}_i & \mathbf{R}_{i-1} & \cdots & \mathbf{R}_1 \\ \mathbf{R}_{i+1} & \mathbf{R}_i & \cdots & \mathbf{R}_2 \\ \vdots & \vdots & \ddots & \vdots \\ \mathbf{R}_{2i-1} & \mathbf{R}_{2i-2} & \cdots & \mathbf{R}_i \end{bmatrix} \quad (2-10)$$

The cov-SSI is a stochastic realization problem aiming at building an observable and controllable model (Van Overschee 1996). To build the model, for a system with order  $n$ , it is necessary to obtain the observability matrix  $\mathbf{O}$  and the controllability matrix  $\mathbf{\Gamma}$  with rank equal to  $n$ . Matrices  $\mathbf{O}$  and  $\mathbf{\Gamma}$  are estimated from the Singular Value Decomposition (SVD) of the Toeplitz matrix ( $\mathbf{T}_{||i}$ ) presented below:

$$\begin{aligned}\mathbf{T}_{||i} &= \mathbf{O}_i \mathbf{\Gamma}_i = \mathbf{U}_1 \mathbf{\Sigma}_1 \mathbf{V}_1^T \\ \mathbf{O}_i &= \mathbf{U}_1 \mathbf{\Sigma}_1^{1/2} \mathbf{M} \\ \mathbf{\Gamma}_i &= \mathbf{M}^{-1} \mathbf{\Sigma}_1^{1/2} \mathbf{V}_1^T\end{aligned}\quad (2-11)$$

In Eq. (2-11)  $\mathbf{U}_1$  and  $\mathbf{V}_1$  are orthogonal matrices consisting of singular vectors,  $\mathbf{\Sigma}_1$  contains the singular values arranged in ascending order, and  $\mathbf{M}$  is assumed to be an identity matrix. After the

determination of  $\mathbf{O}$  and  $\mathbf{\Gamma}$  matrices, many algorithms can be used to determine the discrete state and output matrices ( $\mathbf{A}$  and  $\mathbf{C}$ ) (Hermans and Van Der Auweraer 1999). Once the components of the state space model are determined, the natural frequencies and mode shapes are obtained by performing Eigen Value Decomposition (EVD).

In the cov-SSI analysis, two main parameters should be defined. The first parameter is the time lag. This can be selected by analyzing the PSD diagram and identifying the system's fundamental frequency (Zhou et al. 2022). Based on the sampling frequency ( $f_s$ ) and fundamental frequency ( $f_f$ ), the time lag  $i$  would be:

$$i = 1.5 \frac{f_s}{f_f} \quad (2-12)$$

The order of a system is the second parameter folded by high uncertainty. For this, a value within the range of 4 to 30 times the desired number of modes is suggested (Wu, Wen-Hwa et al. 2016). Plotting and interpreting a stabilization diagram is inevitable since the model's order is usually overestimated. In the stabilization diagram, the following errors for stability criteria are defined (Lee et al. 2018):

$$\begin{aligned} \text{Frequency: } & \frac{|f^{(p+1)} + f^{(p)}|}{f^{(p)}} \times 100\% < 1\% \\ \text{Damping ratio: } & \frac{|\xi^{(p+1)} + \xi^{(p)}|}{\xi^{(p)}} \times 100\% < 5\% \\ \text{Mode shape: } & 1 - \text{MAC}(\phi^p, \phi^{p+1}) \times 100\% < 3\% \end{aligned} \quad (2-13)$$

In Eq. (2-13)  $f$ ,  $\xi$ , and  $\phi$  are the natural frequencies, damping ratios, and mode shapes, respectively. The parameter  $p$  denotes the system order, and MAC is the modal assurance criterion between derived mode shapes. The MAC of two vectors ( $\mathbf{a}$ ,  $\mathbf{b}$ ) can be calculated from the following relation:

$$\text{MAC}(\mathbf{a}, \mathbf{b}) = \frac{|\mathbf{a}^T \mathbf{b}|^2}{\mathbf{a}^T \mathbf{a} \mathbf{b}^T \mathbf{b}} \quad (2-14)$$

In the current study, a MATLAB script is adopted to perform the cov-SSI analysis.

### 2.3. Traditional Frequency Domain Decomposition

Based on the theories related to stochastic processes, the relation between two realizations can be defined by a Correlation Function (CF) matrix. It is comprised of diagonal elements as the autocorrelations and non-diagonals as cross-correlations. For the Gaussian signals or close ones, the correlation function contains significant properties if and only if they are stationary, and ergodic, with a mean value equal to zero. In the vibrational analysis, the components of the CF matrix for two random signals of  $x(t)$  and  $y(t)$  are defined as:

$$\begin{aligned} R_x(\tau) &= E[x(t)x(t+\tau)] \\ R_y(\tau) &= E[y(t)y(t+\tau)] \\ R_{xy}(\tau) &= E[x(t)y(t+\tau)] \end{aligned} \quad (2-15)$$

Where  $E$  represents the expectation and using the time averaging technique, it has the integral form of:

$$\begin{aligned} R_x(\tau) &= \frac{1}{T} \int_0^T x(t)x(t+\tau)dt \\ R_y(\tau) &= \frac{1}{T} \int_0^T y(t)y(t+\tau)dt \\ R_{xy}(\tau) &= \frac{1}{T} \int_0^T x(t)y(t+\tau)dt \end{aligned} \quad (2-16)$$

In the Eq. (2-16), the parameter  $T$  is the time interval. Since it is assumed that the signal is stationary, the shift in the integral's time bounds is allowed. This leads to the derivation of the convolution integral presented in Eq. (2-17).

$$\begin{aligned}
R_x(\tau) &= \frac{1}{T} \int_{-T-\tau}^{-\tau} x(-\theta-\tau)x(-\theta)d\theta = \frac{1}{T} \int_0^T x(-\theta)x(\tau-\theta)d\theta = x(-t) * x(t) \\
R_y(\tau) &= \frac{1}{T} \int_{-T-\tau}^{-\tau} y(-\theta-\tau)y(-\theta)d\theta = \frac{1}{T} \int_0^T y(-\theta)y(\tau-\theta)d\theta = y(-t) * y(t) \\
R_{xy}(\tau) &= \frac{1}{T} \int_{-T-\tau}^{-\tau} x(-\theta-\tau)y(-\theta)d\theta = \frac{1}{T} \int_0^T x(-\theta)y(\tau-\theta)d\theta = x(-t) * y(t)
\end{aligned} \tag{2-17}$$

In Eq. (2-17), the integral variable is changed. At this point, it is proven that the correlation function is the convolution of the two signals. In addition, the autocorrelation represents the free decay of motion for an SDOF system.

To investigate the power distribution in the frequency domain, the Fourier transform of the correlation function is often performed. As a result, the PSD matrix will consist of diagonal and non-diagonal elements which are calculated by the Fourier transform of auto and cross-correlations respectively. Thus, the PSD matrix elements have the form of:

$$\begin{aligned}
G_{xx}(\omega) &= X(-\omega)X(\omega) = X^*(\omega)X(\omega) \\
G_{yy}(\omega) &= Y(-\omega)Y(\omega) = Y^*(\omega)Y(\omega) \\
G_{yx}(\omega) &= Y(-\omega)X(\omega) = Y^*(\omega)X(\omega)
\end{aligned} \tag{2-18}$$

It is worthwhile to state that in the derivation process, the reversal property of Fourier transform is used in which the  $X(-\omega)$  becomes  $X^*(\omega)$  (complex conjugate). Referring to the classical structural dynamics, the Fourier transform of the response is equal to the Fourier transform of input acceleration multiplied by the Frequency Response Function (FRF). This is indicated in Eq. (2-19) where H represents FRF. Thus, by replacing the Fourier transform of the response in Eq. (2-18), the PSD of output would be:

$$\begin{aligned}
Y(\omega) &= X(\omega)H(i\omega) \\
G_{yy}(\omega) &= Y^*(\omega)Y(\omega) = X^*(\omega)X(\omega)H^*(i\omega)H(i\omega) = G_{xx}(\omega)H^*(i\omega)H(i\omega) = G_{xx}(\omega) |H(i\omega)|^2
\end{aligned} \tag{2-19}$$

In addition, by recalling the integral form of the convolutions, the same relation can be established for the PSD of the output. The above relation is the fundamental theorem for stationary signals where the PSD of output is a function of the input counterpart.

The problem formulation is approximated based on the following assumptions: the input of the ambient vibration is accepted as white noise; the modal coordinates are uncorrelated. In theory, the FRF can be written as the summation of:

$$H(i\omega) = \sum_{k=1}^n \left( \frac{R_k}{(i\omega - \lambda_k)} + \frac{R_k^*}{(i\omega - \lambda_k^*)} \right) \quad (2-20)$$

In which  $n$ ,  $\lambda_k$ ,  $R_k$  and  $R_k^*$  are the numbers of modes, pole, residue, and its complex conjugate respectively. As stated, the simplification is made by assuming the input as a white noise signal. This assumption results in considering the correlation of the input signal ( $R_{xx}$ ) as Dirac's delta while its Fourier transform ( $G_{xx}$ ) would be a scalar value ( $C$ ). Therefore, Eq. (2-19) becomes:

$$G_{yy}(i\omega) = \sum_{k=1}^n \sum_{s=1}^n \left[ \frac{R_k}{(i\omega - \lambda_k)} + \frac{R_k^*}{(i\omega - \lambda_k^*)} \right] C \left[ \frac{R_s}{(i\omega - \lambda_s)} + \frac{R_s^*}{(i\omega - \lambda_s^*)} \right] \quad (2-21)$$

Conducting a detailed mathematical manipulation explicitly written in the reference (Brincker n.d.) while assuming that the  $k$ th residue of the output PSD is proportional to the mode shape vector in the lightly damped systems, the PSD of the output will be written as:

$$G_{yy}(i\omega) = \sum_{k \in \text{sub}(\omega)} \left( \frac{d_k \phi_k \phi_k^T}{i\omega - \lambda_k} + \frac{d_k^* \phi_k^* \phi_k^{*H}}{i\omega - \lambda_k^*} \right) \quad (2-22)$$

Where  $d$  is the scalar constant,  $\phi$  is the mode shape vector, and  $\phi_k^{*H}$  is the complex conjugate of its transpose. The above relation is the approximate solution for the PSD of the output.

In the power spectral density of the outputs, each peak represents the dominance of a mode or its combination with close ones. If only one mode dominates, the summation indicated in Eq.(2-22) has only one term (Brincker et al. n.d.), (Brincker n.d.). To obtain the modal properties from that term near the peak, it is suggested to use the SVD technique to decompose the PSD. SVD can be considered a powerful technique in comparison with Eigen Value Decomposition (EVD). For instance, to obtain orthogonal mode shapes of matrix  $\mathbf{A}$  using EVD, several

mathematical properties such as being symmetrical and rectangular must be satisfied which is not necessary for the SVD. To elaborate the method, the decomposition involves finding the best fitting subspace for a set of data scattered in the  $k$  dimension. In other words, assuming a set of data in 2 dimensions, the best fitting line with the least vertical distance from the data can be obtained by maximizing the projection length or minimizing the square distance. Then, the algorithm of this best-fitting line with the least square distance is further developed for the  $k$  lines to build the subspace fitting the data in the  $k$  dimension. Assuming  $G_{yy}(i\omega_i)$  as the power spectral density at discrete frequencies, its SVD decomposition has the form of:

$$G_{yy}(i\omega_i) = U_i S_i V_i^H \quad (2-23)$$

Where  $\mathbf{S}$  is the ordered first singular values and  $\mathbf{U}$ , and  $\mathbf{V}$  are the corresponding first singular vectors. After determination of singular values, the SV spectrum is formed. At this stage, the expert select the peaks in the SV spectrum representing modes with prominent vibration. The corresponding singular vectors are considered as the mode shapes.

#### 2.4. Automated Frequency Domain Decomposition

In the traditional FDD, after the derivation of the SV spectrum, there is a need for manual selection of peaks representing physical modes of vibration. Therefore, automating the peak-picking mechanism is necessary to address this limitation of the traditional FDD procedure. This challenge becomes even more pronounced when dealing with closely spaced modes of vibration and spurious peaks in the SV spectrum. The following algorithm for AFDD is introduced, drawing inspiration from previous work by Brincker:

1. Set the AFDD hyper-parameters
  - a. Number of desired modes to be identified.
  - b. Frequency range of interest.

- c. The  $\alpha$  threshold distinguishing between different modes of vibration.
  - d. The number of points to be considered over the modal domain assessment.
  - e. Mean MAC value for modal domain assessment and validation of physical mode.
2. Identify the first peak in the SV spectrum.
  3. Calculate the MAC between the singular vector of the selected peak and the vectors corresponding to other SV values.
  4. Remove the SV points with the calculated MAC above the  $\alpha$  threshold, as they correspond to the identified mode.
  5. Perform the modal domain assessment to validate the presence of a physical mode.
  6. Select the next peak in the SV spectrum until reaching the predefined number of desired modes.

The above algorithm is illustrated in the flowchart of Fig. 2-1.

In summary, the first step in implementing the AFDD consists of defining the frequency range of interest and the number of desired modes within that range. Then, the presented algorithm selects a peak in the SV spectrum, and the points with a similar vibrational mode are filtered out from the peak-picking process to handle spurious peaks. In this regard, the MAC between the selected peak mode shape and vectors associated with other SVs is determined. Other SV peaks having the MAC below the predefined threshold are included in the peak-picking process to identify a proceeding one. At this stage, the evaluation of the modal domain initiates, in which the SVs with a MAC above the predefined threshold are analyzed. Domain assessment involves verifying the gradual variation of MAC from the predefined threshold ( $\alpha$ ) to 1 around a peak in the spectrum and ensures the presence of a physical mode shape.

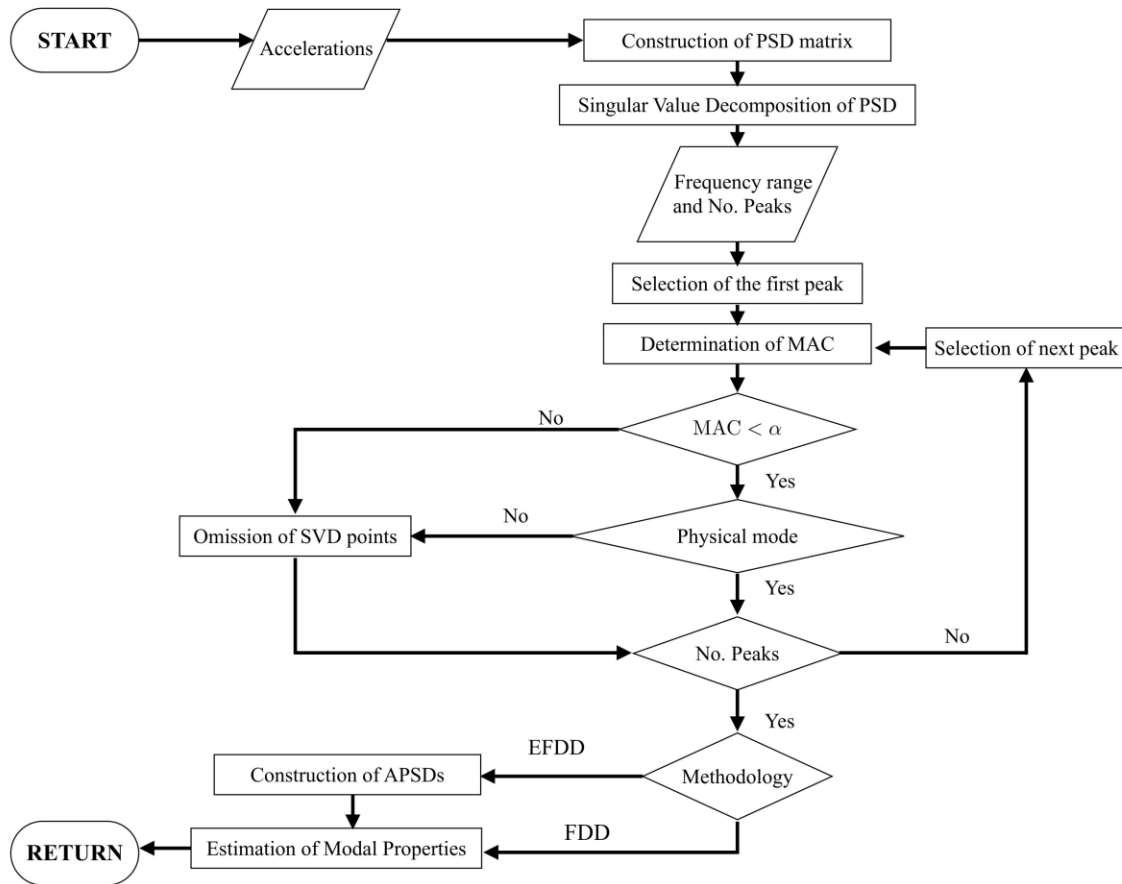


Fig. 2-1. The flowchart of the AFDD algorithm.

In this study, a script is developed based on the above formulation. The extracted modal properties are limited to the natural frequencies and mode shapes since, similar to the manual EFDD, its automated version results in inaccurate estimation of damping ratios (Qu et al. 2023).

### 3. OPTIMIZATION OF AUTOMATED FREQUENCY DOMAIN DECOMPOSITION

Since several factors affect the accuracy of the frequencies estimated by the AFDD methodology, a sensitivity analysis is performed using the experimental data from the Yonghe cable-stayed bridge to acquire AFDD's optimal performance. It results in introducing universal hyper-parameters and subsides the need for further tuning of them for each case study. The considered input data is the ambient vibration response recorded on January 17, 2008, from 9:00 pm to 12:00 am.

#### 3.1. Description of SHM benchmark

The Yonghe cable-stayed bridge was built in 1983 and is located in the port of Tianjin, Hebei province, China. The SHM benchmark is constructed with a length and width of 510 and 11 m. It consists of a 210-meter main span and two 125-meter secondary spans. The bridge deck is connected to the north and south towers by 88 pairs of 5 mm cables. An advanced monitoring system at the HIT infrastructure center was designed for monitoring while being retrofitted in 2005-2007. The SHM system includes more than 150 sensors from which 14 uniaxial accelerometers are mounted on the deck (Li et al. 2014), as illustrated in Fig. 3-2.



Fig. 3-1. The Yonghe cable stayed bridge in China.

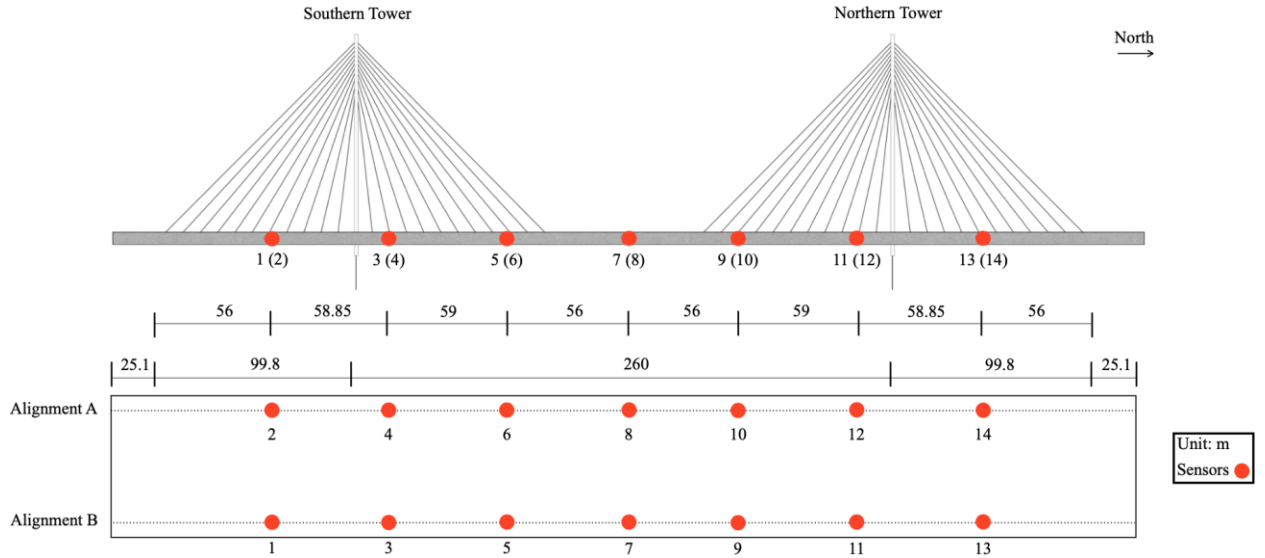


Fig. 3-2. The SHM configuration proposed for the Yonghe cable-stayed bridge.

In the sensitivity analysis to define the optimal MAC threshold, the calibrated 3D Finite Element (FE) model of the bridge was used to identify the target frequencies. The FE model was developed in ANSYS Mechanical APDL. The main girders and towers were modeled using the three-dimensional beam element (BEAM 44), while the mass elements and linear elastic links (LINK 10) were assigned to the transverse beams and cables, respectively. All boundary conditions were defined accordingly, including the rubber supports, which are displayed in Fig. 3-3.

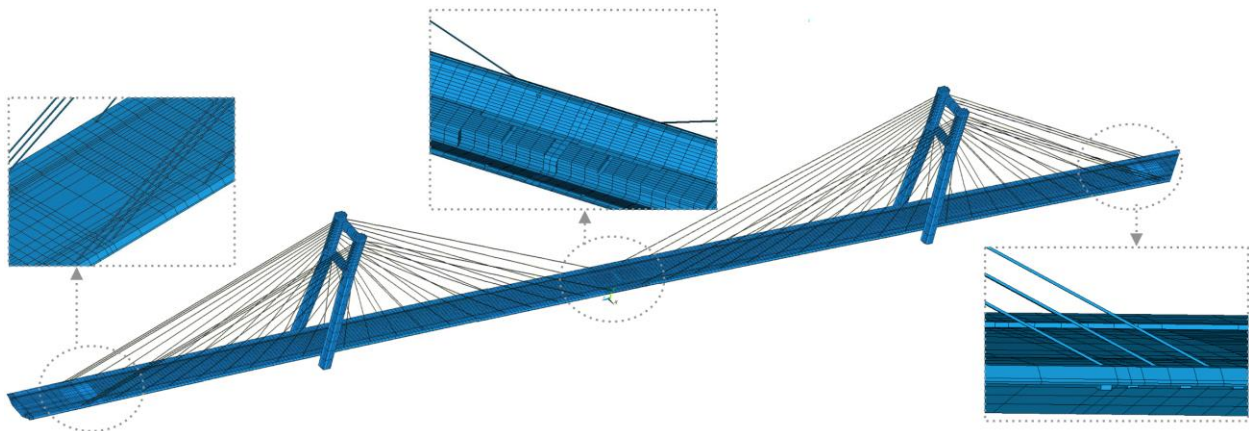


Fig. 3-3. FE model of the Yonghe cable-stayed.

### 3.2. Preprocessing of input

The raw acceleration time histories were preprocessed with Hanning window filtering to remove spikes and irregular trends. Additionally, the records were filtered through a six-order Butterworth bandpass with low and high-frequency cuts of 0.1 and 30 Hz (García-Macías and Ubertini 2021). A baseline correction was then performed using OpenSeisSignal (Papazafeiropoulos and Plevris 2018).

Two approaches based on the discrete wavelet transform and SVD exist to filter the contaminated records in the field of signal processing. The latter performs better in noise filtering from ambient vibration response, while the former exhibits better denoising capacity for recorded seismic signals. In the denoising process based on the SVD, a matrix of rank  $r$  comprised of the contaminated signals is truncated, assuming the presence of singular values equal to zero, as written below:

$$\mathbf{Y} = \mathbf{U}_r \mathbf{U}_{m-r} \begin{bmatrix} \mathbf{S}_r & 0 \\ 0 & 0 \end{bmatrix} \begin{bmatrix} \mathbf{V}_r^T \\ \mathbf{U}_{n-r}^T \end{bmatrix} = \mathbf{U}_r \mathbf{S}_r \mathbf{V}_r^T \quad (3-1)$$

In which  $\mathbf{U}_r$  and  $\mathbf{V}_r$  are orthogonal matrices related to singular vectors, and  $\mathbf{S}_r$  is its corresponding matrix with singular values as the diagonal elements. The methodology consists of the following steps:

Step 1. Generating a Hankel matrix  $\mathbf{Y}$  with dimensions  $(m, n)$  from the signal  $\mathbf{y}$ :

$$\mathbf{Y}_{m,n} = \begin{bmatrix} y_1 & y_2 & \cdots & y_n \\ y_2 & y_3 & \cdots & y_{n+1} \\ \vdots & \vdots & \ddots & \vdots \\ y_m & y_{m+1} & \cdots & y_N \end{bmatrix} \quad (3-2)$$

Step 2. Dividing the Hankel matrix into a healthy  $(\mathbf{X}_{m,n})$  and a noisy subspace  $(\mathbf{N}_{m,n})$ :

$$\mathbf{Y}_{m,n} = \mathbf{X}_{m,n} + \mathbf{N}_{m,n} \quad (3-3)$$

Step 3. Denoising the signal by decomposing the structured Hankel matrix  $\mathbf{Y}$  using the SVD combined with subsequence truncation of small SVs:

$$\mathbf{Y}_{m,n} = \sum_{i=1}^m s_i \mathbf{u}_i \mathbf{v}_i^T = \sum_{i=1}^l s_i \mathbf{u}_i \mathbf{v}_i^T + \sum_{i=l+1}^m s_i \mathbf{u}_i \mathbf{v}_i^T = \mathbf{X}_{m,n} + \mathbf{N}_{m,n} \quad (3-4)$$

$$s_1 > s_2 > \dots > s_l \gg s_{l+1} = s_{l+2} = \dots = s_m \approx 0$$

In which  $s_i, \mathbf{u}_i, \mathbf{v}_i^T$  are the singular values and corresponding singular vectors, respectively. In addition,  $l$  and  $m$  are parameters that affect the process and are determined for optimal denoising.

Step 4. Construction of corresponding denoised signal vector with  $\bar{x}_i$  elements from the non-Hankel noise-free matrix using arithmetic averaging of anti-diagonal elements (Sanliturk and Cakar 2005):

$$\mathbf{X}_{m,n} = \begin{bmatrix} \hat{x}_1 & \hat{x}_2 & \dots & \hat{x}_n \\ \hat{x}_2 & \hat{x}_3 & \dots & \hat{x}_{n+1} \\ \vdots & \vdots & \ddots & \vdots \\ \hat{x}_m & \hat{x}_{m+1} & \dots & \hat{x}_{N-1} \end{bmatrix} \quad (3-5)$$

$$\bar{x}_i = \frac{1}{k-l+1} \sum_{j=l}^k \mathbf{X}_{i-j+1,j}$$

$$l = \max(1, i - m + 1)$$

$$k = \min(n, i)$$

As indicated, there are two main parameters affecting the SVD filter accuracy. For the ambient vibration signals, it was considered  $m=300$  and  $l=5\%$  of the first singular value for optimal denoising performance, according to (Ravizza et al. 2021).

### 3.3. Sensitivity analysis

The proposed procedure must offer an effective hyperparameter without requiring further tuning to estimate modal properties accurately under different conditions affecting structural behavior. Furthermore, an effective MAC threshold ( $\alpha$ ) should be defined to distinguish between different modes present in a system and establish optimal performance for the AFDD. There are

additional factors that can significantly affect the extracted natural frequencies obtained from the AFDD algorithm, including:

- The acceleration length.
- The noise level affecting the input signal.
- The spatial resolution formed by sensors in a monitoring system.
- The desired number of modes within the prescribed frequency range.

In this regard, values in the range of 0 to 1 are assigned to the MAC threshold, investigating its impact on the extracted modal properties through several sensitivity analyses. Stabilization diagrams are constructed throughout the sensitivity analyses, in which the modal frequencies obtained from the AFDD method are compared with the reference values taken from the FE model. Proper ranges associated with the  $\alpha$  threshold are obtained through the stabilization diagrams, resulting in optimal AFDD performance. Additionally, three distinct regions are identified based on the number of misidentified modes: unstable, sub-optimal, and optimal regions within the diagram. In this regards, the GMM algorithm is utilized to define a core and an outlier cluster in each stabilization diagram. The algorithm considers the difference between the AFDD estimate and its FE counterpart. It classifies the frequencies into the core cluster if the difference is below the defined margin. The margin is set as 0.1 Hz and points exceeding this margin are included in the outlier one. Consequently, over the sensitivity analysis, the number of frequencies present in each cluster is determined for each MAC threshold  $\alpha$ . If all of the AFDD estimates fall inside the core cluster, the optimal region is assigned to its corresponding  $\alpha$  value. In the case of one estimated frequency in the outlier cluster, the corresponding  $\alpha$  value falls into the suboptimal region. The unstable region includes all  $\alpha$  values which result in the more than one AFDD estimates inside the outlier cluster.

Before initiating the analysis, the frequency range of interest and number of desired modes are specified. According to the outputs from the FE model, there are seven modes in the frequency range of 0-1.5 Hz that should be identified, except for a sensitivity case where the number of desired modes is variable.

It is worth noting that during the sensitivity analysis, the assessment of the modal domain, which prevents the selection of non-physical modes, is deactivated. Due to the direct influence of the optimal  $\alpha$  in modal domain assessment, this decision is made to comprehensively evaluate the effect of each influential factor and  $\alpha$  variation on extracted properties and determine the MAC optimal threshold primarily.

In the first sensitivity analysis, the MAC threshold  $\alpha$  varies from 0 to 1 in the increments of 0.02. Thus, the AFDD analysis was repeated 50 times by fixing  $\alpha$  value. The identified frequencies are compared with the FE results in the stabilization diagram of Fig. 3-4. In the graph, the AFDD frequency estimates are reported on the x-axis, while the y-axis represents the selected MAC's thresholds. The FE model target frequencies are 0.42 Hz, 0.6 Hz, 0.88 Hz, 1.04 Hz, 1.09 Hz, 1.21 Hz, and 1.44 Hz, indicated by vertical solid lines.

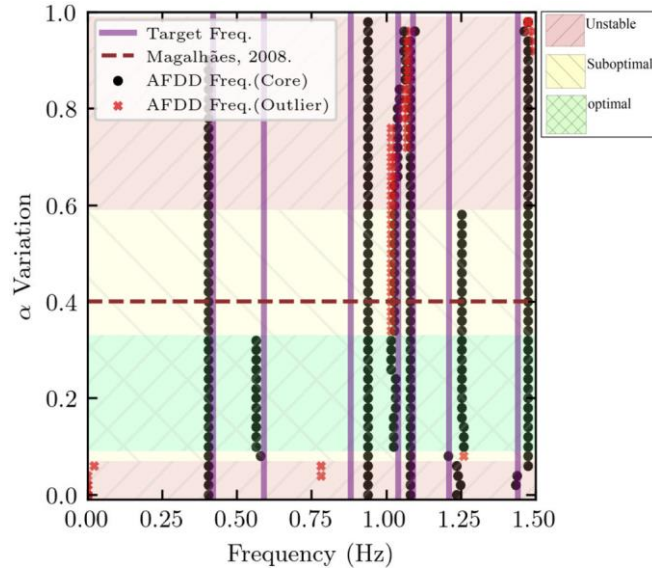
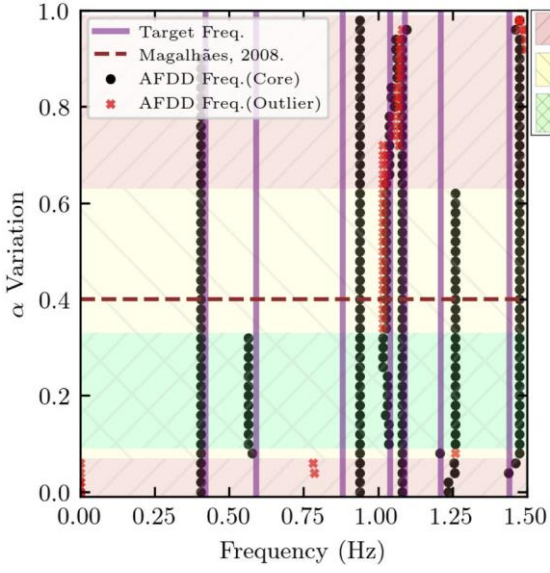


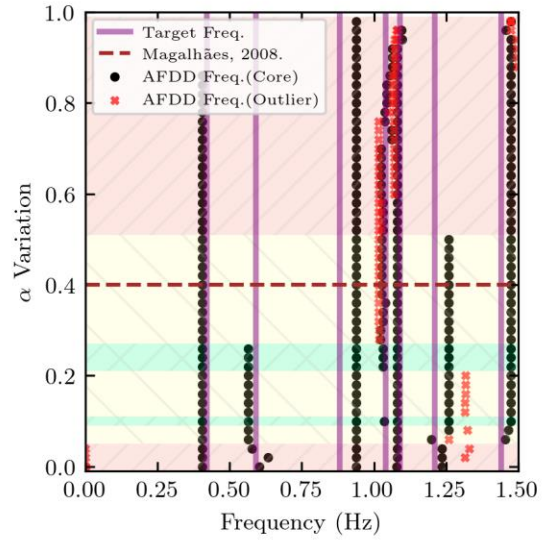
Fig. 3-4. The effect of  $\alpha$  variation on the AFDD's outcomes.

As it is seen, the target frequencies at 0.42 Hz, 0.88 Hz, and 1.44 Hz could be identified for almost any  $\alpha$  Value. Conversely, 1.04 Hz and 1.09 Hz frequencies were affected by the MAC threshold variation as other frequencies with different values were picked by the algorithm, particularly for  $\alpha$  above 0.6. In this sensitivity analysis, the optimal area, where almost all frequencies are estimated accurately, falls within the range of  $\alpha$  from 0.10 to 0.34. Remarkably, the suggested value of  $\alpha = 0.4$  by (Magalhães et al. 2008a), highlighted in the graph with a horizontal solid line, falls within the suboptimal region and would have led to neglecting the 0.6 Hz frequency.

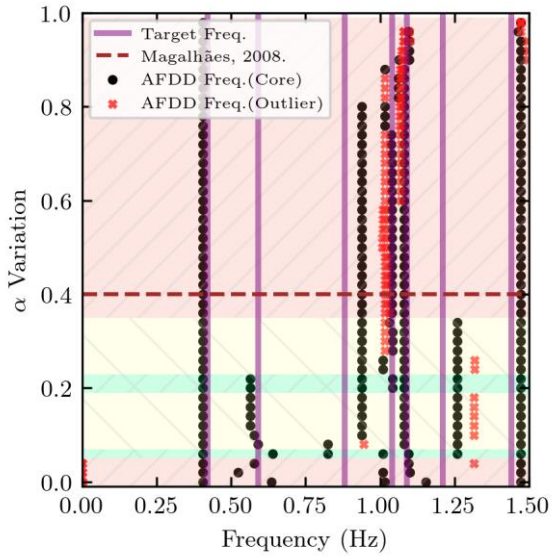
In the second sensitivity analysis, the effect of different noise levels was investigated. Increasing the hyper-parameter  $l$  in the denoising mechanism leads to higher noise levels in the output signal. Five cases were considered, setting the  $l$  hyper-parameter to 0.05, 0.20, 0.35, 0.50, and 0.75.



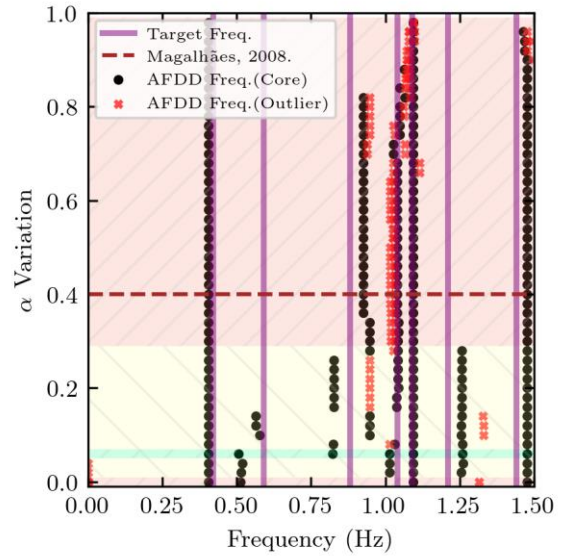
(a)



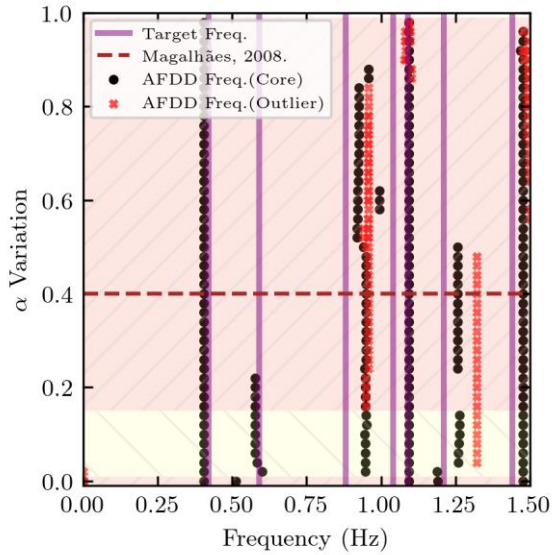
(b)



(c)



(d)

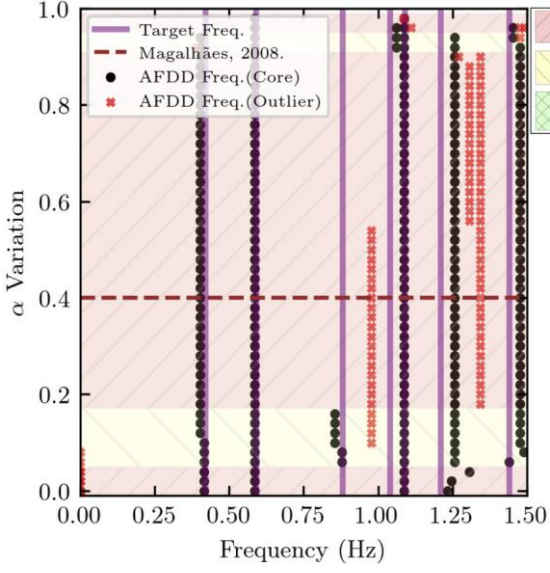


(e)

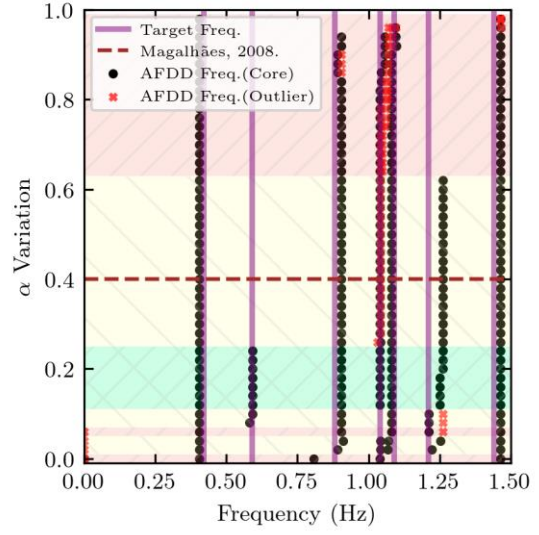
Fig. 3-5. The effect of  $\alpha$  variation with the noise level: (a) SVD denoising parameter  $l=0.05$ , (b)  $l=0.20$ , (c)  $l=0.35$ , (d)  $l=0.50$ , (e)  $l=0.75$ .

Fig. 3-5 reveals that the regions of optimal and sub-optimal shrink as the noise level increases. In fact, when  $l=0.50$  and  $l=0.75$ , it is no longer possible to define an optimal region where all modes are detected. Modes with target frequencies of 0.88 Hz and 1.04 Hz were the modes highly affected by noise and  $\alpha$  variation. When  $l=0.05$ , optimal denoising is achieved, and the optimal region is delimited by a MAC threshold ranging from 0.18 to 0.22.

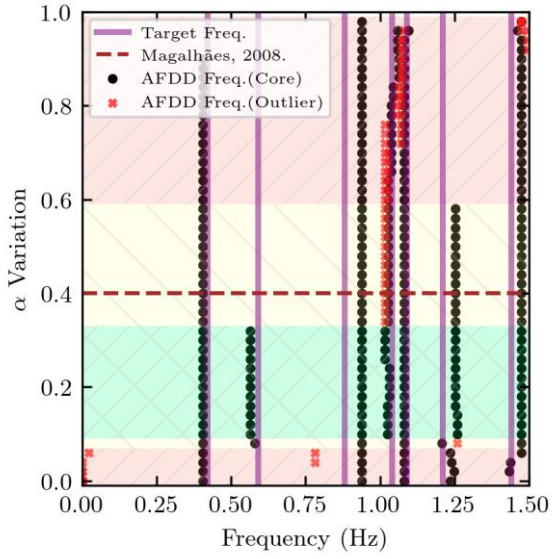
The third sensitivity analysis investigates the effect of the acceleration records' length. The first natural period of the Yonghe cable-stayed bridge is about 2.40 s. It is recommended to consider a signal length exceeding 1000-2000 times the first natural period of the system (Cantiene 2004). Moreover, the 15 to 60 minutes signals exhibited accurate results in the dynamic characterizations (Pereira et al. 2021). The proper signal length is proportional to damping, noise-to-signal ratio, and the characterization method. Consequently, the effect of  $\alpha$  variation is analyzed for signals with the following lengths: 5 minutes, 1, 4, 12, and 24 hours (Fig. 3-6).



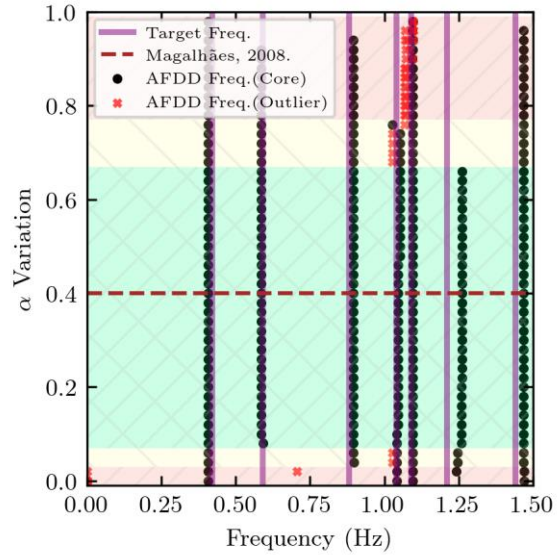
(a)



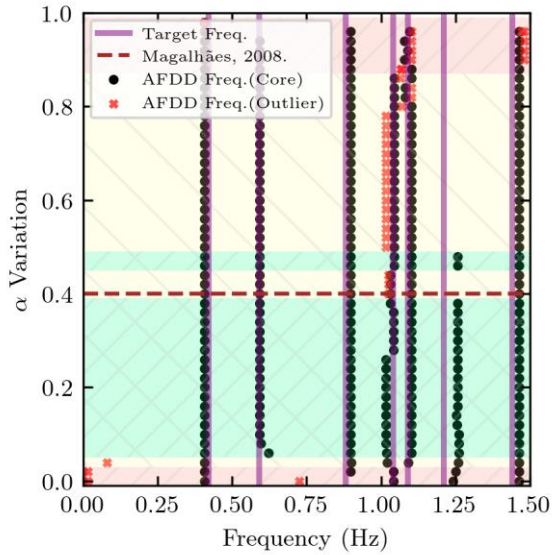
(b)



(c)



(d)



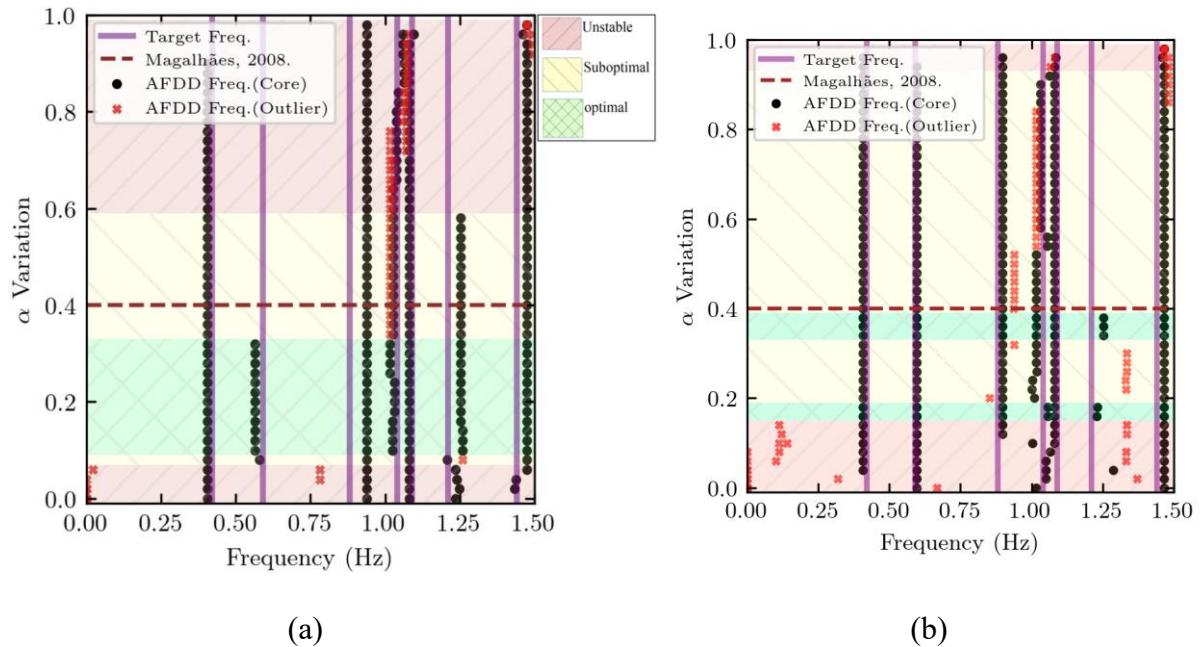
(e)

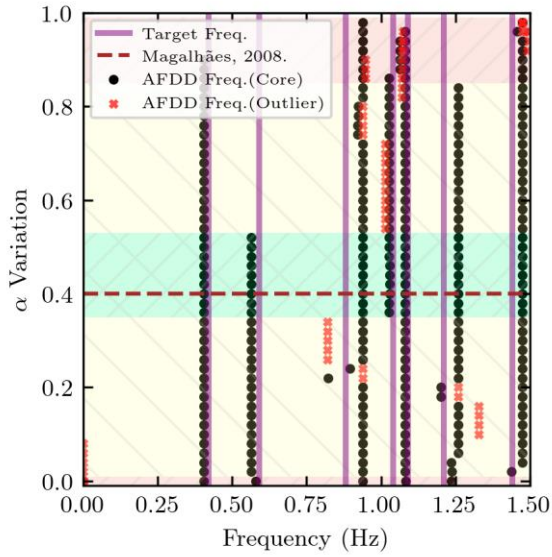
Fig. 3-6. The effect of  $\alpha$  variation and signal length: Input duration of (a) 5 minutes, (b) 1 hour, (c) 4 hours, (d) 12 hours, (e) 24 hours.

Commonly, longer signal durations offer a more comprehensive dataset to capture the dynamic characteristics of a structure, leading to more reliable frequency estimations. Indeed, as demonstrated in Fig. 3-6, the optimal region widens as the signal length increases, and the most inaccurate results correspond to a 5-minute duration. As indicated in Fig. 3-6.b and Fig. 3-6.c, although the optimal region widens, the precision of estimating the target frequency of 0.59 Hz decreases. The reason attributes to the ambient vibration characteristics and the excitation level during that period. Nonetheless, the analysis shows that by selecting an appropriate  $\alpha$  value, it is possible to obtain accurate results with 1-hour records. This approach could be helpful in designing monitoring campaigns, potentially reducing their cost by determining a proper duration.

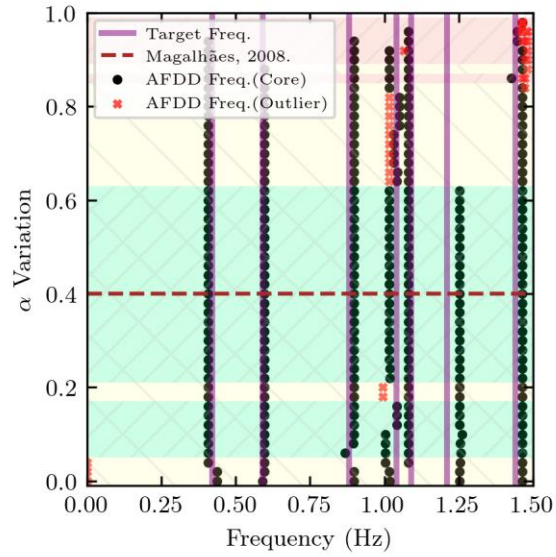
In a monitoring campaign, the sensor layout is of paramount importance due to its direct impact on mode shape estimations. Thus, the fourth sensitivity analysis evaluates the effect of reducing the number of sensors and changing their location. To this end, four different sensor configurations were considered besides the original layout. As shown in Fig. 3-7.f, only the sensors

located on alignment A were placed in layouts 1 and 4, while other arrangements were formed by omitting different sensors on both alignments. For the first layout, the obtained results didn't comply with the expected optimal and suboptimal regions. Two factors might have contributed to this issue: 1) this layout was parallel to the mid-span axis considered during the FE modal analysis. 2) the presence of malfunctioning sensors. Further discussion is made in the following section about sensor health. Since the AFDD relied on modal geometry, the optimal MAC threshold depended on the sensor's spatial resolution. This fact was noticeable when analyzing the scenario with only three sensors on alignment A, as depicted in Fig. 3-7.f. In this case, any MAC threshold led to inaccurate results (Fig. 3-7 e). Nonetheless, it is worth noting that across all layouts, the modes with target frequencies of 0.42 Hz and 1.44 Hz are less sensitive to the system spatial resolution and can always be detected. This observation is mainly due to the higher mass participation factors of these modes.

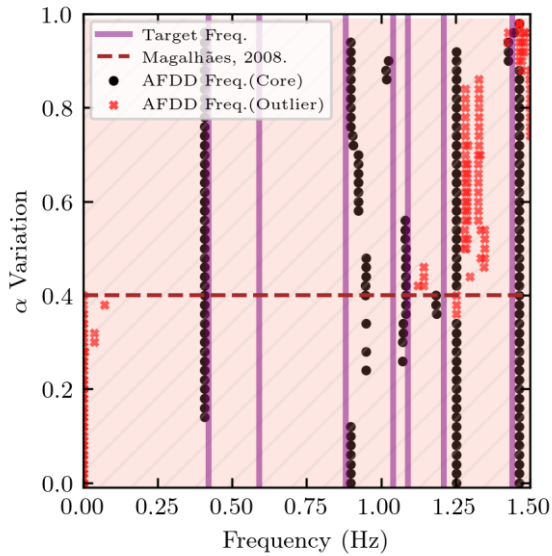




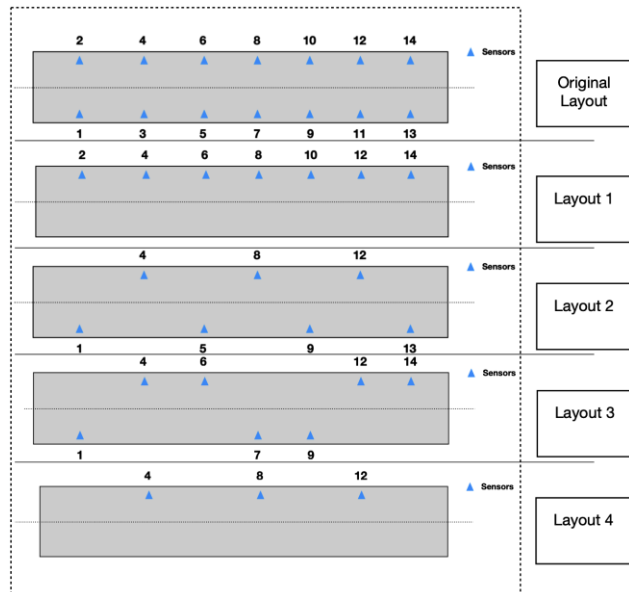
(c)



(d)



(e)

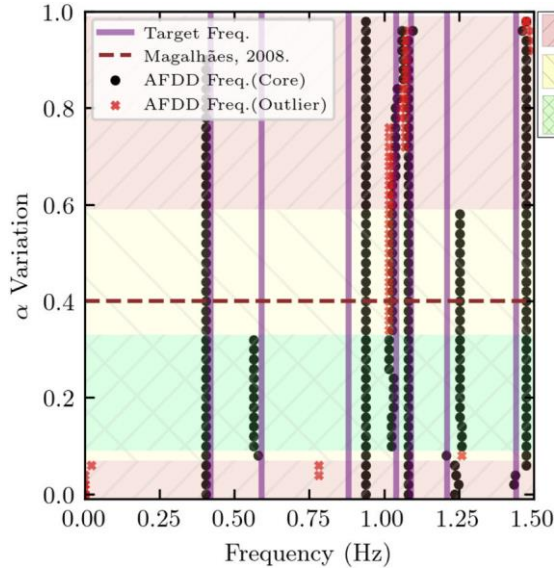


(f)

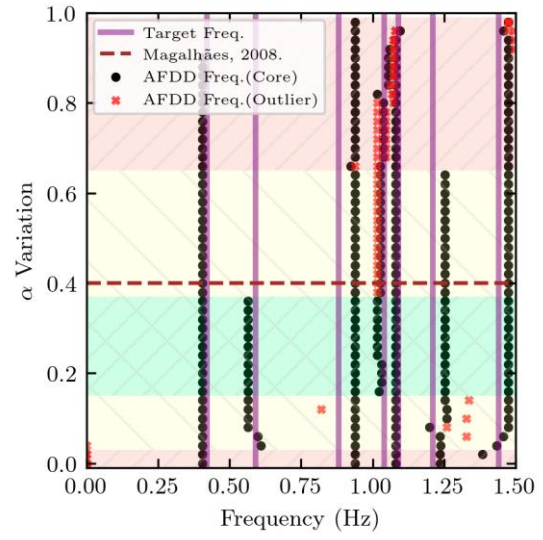
Fig. 3-7. The effect of  $\alpha$  variation with the number of sensors, and their configuration: (a) original layout, (b) layout 1, (c) layout 2, (d) layout 3, (e) layout 4, (f) sensors layout.

The number of existing modes within a frequency range is often unknown in the modal identification tasks. Besides, the sampling frequency varies among case studies based on the data acquisition systems. In this regard, the sampling frequency and the number of desired output

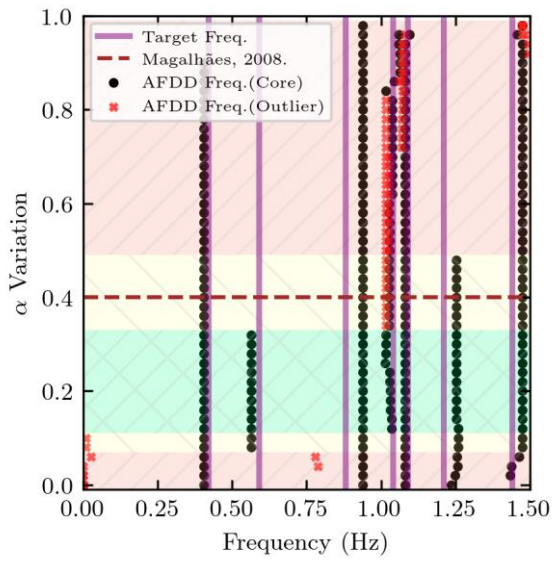
frequencies are additional influential factors in the sensitivity analysis. As illustrated in Fig. 3-8, It was found that the optimal region is barely affected by the sampling frequency change.



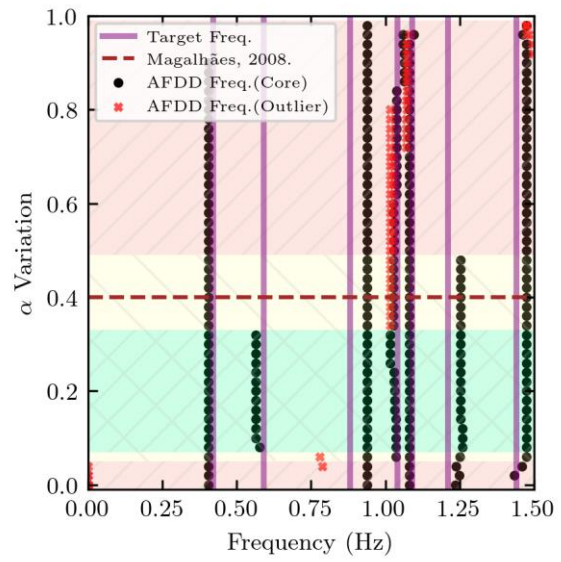
(a)



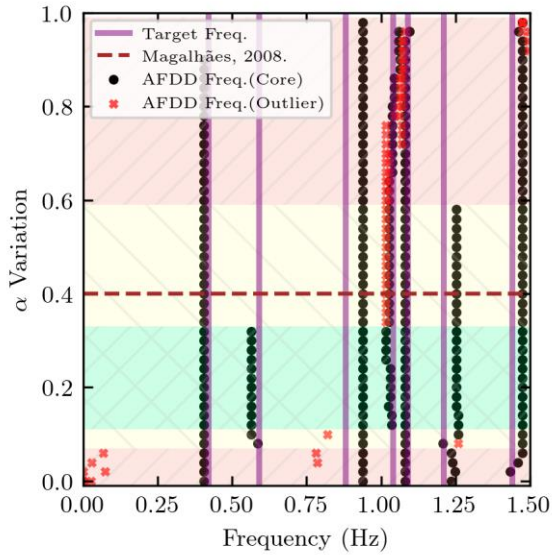
(b)



(c)



(d)



(e)

Fig. 3-8. The effect of MAC variation with sampling frequency on the AFDD outcomes: Sampling frequencies of (a)  $F_s=100$  Hz, (a)  $F_s=100$  Hz, (b)  $F_s=20$  Hz, (c)  $F_s=150$  Hz, (d)  $F_s=300$  Hz, (e)  $F_s=400$  Hz.

Regarding the number of desired output frequencies, the sensitivity analysis considered 2, 4, 7, and 9 output values. The results presented in Fig. 3-9 disclose that when the desired output frequencies are fixed less than the present ones within a frequency range, the optimal region widens, and the algorithm identifies modes with higher mass participation factors. Furthermore, for the case of 9 desired modes, modes with zero-valued natural frequency are observed for the  $\alpha$  value below 0.2.

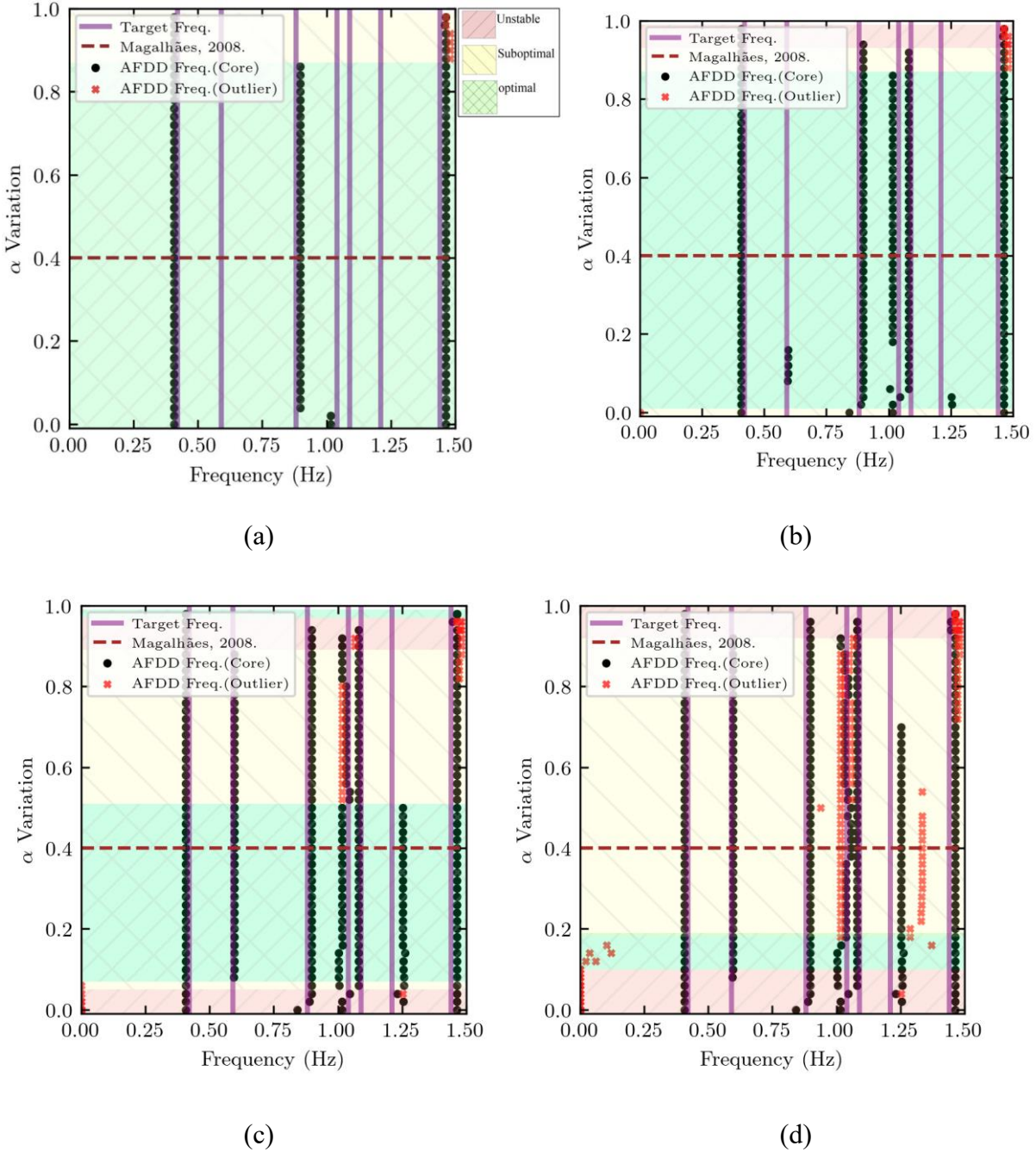


Fig. 3-9. The effect of MAC variation and number of required peaks on the AFDD outcomes: (a) No. peak is 3, (b) No. peak is 5, (c) No. peak is 7, (d) No. peak is 9.

A qualitative plot illustrating the accuracy of AFDD estimates across all analyses is presented in Fig. 3-10. For each value of  $\alpha$  in the horizontal axis, the AFDD outcomes are compared to the target frequencies and deemed correct if the difference is less than 0.1 Hz. Then,

the number of correct estimations is divided by the total AFDD analyses to derive a ratio between 0-1. This ratio is denoted as the ratio of correct estimation on the y-axis while the x-axis indicates the corresponding  $\alpha$  value.

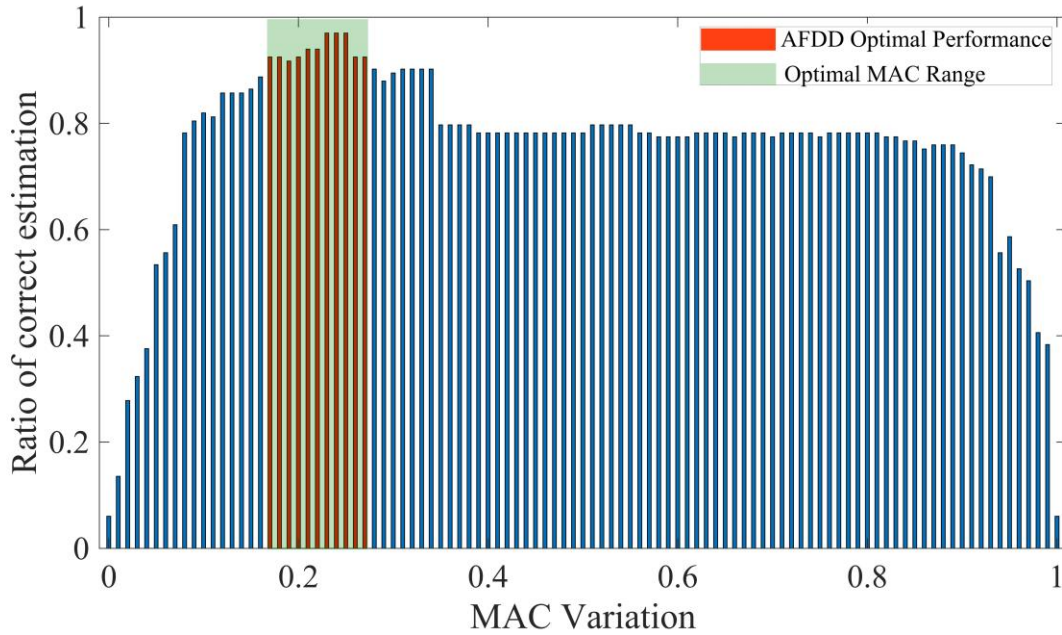


Fig. 3-10. Qualitative correct estimation for each  $\alpha$  value.

Fig. 3-11. summarizes the optimal and suboptimal regions for different scenarios in the sensitivity analyses. The analysis revealed that the AFDD reaches optimal performance by assuming the MAC's threshold in the range of 0.18-0.24. Accordingly, in the following sections, the proposed AFDD methodology is applied to three case studies considering a MAC threshold of  $\alpha = 0.2$ . This value differs from the previous findings of (Magalhães et al. 2008b), where the suggested MAC threshold was set at 0.4. Therefore, based on the sensitivity analysis results, the obtained optimal  $\alpha$  should be considered, and values from the literature are not confirmed for the adapted algorithm.

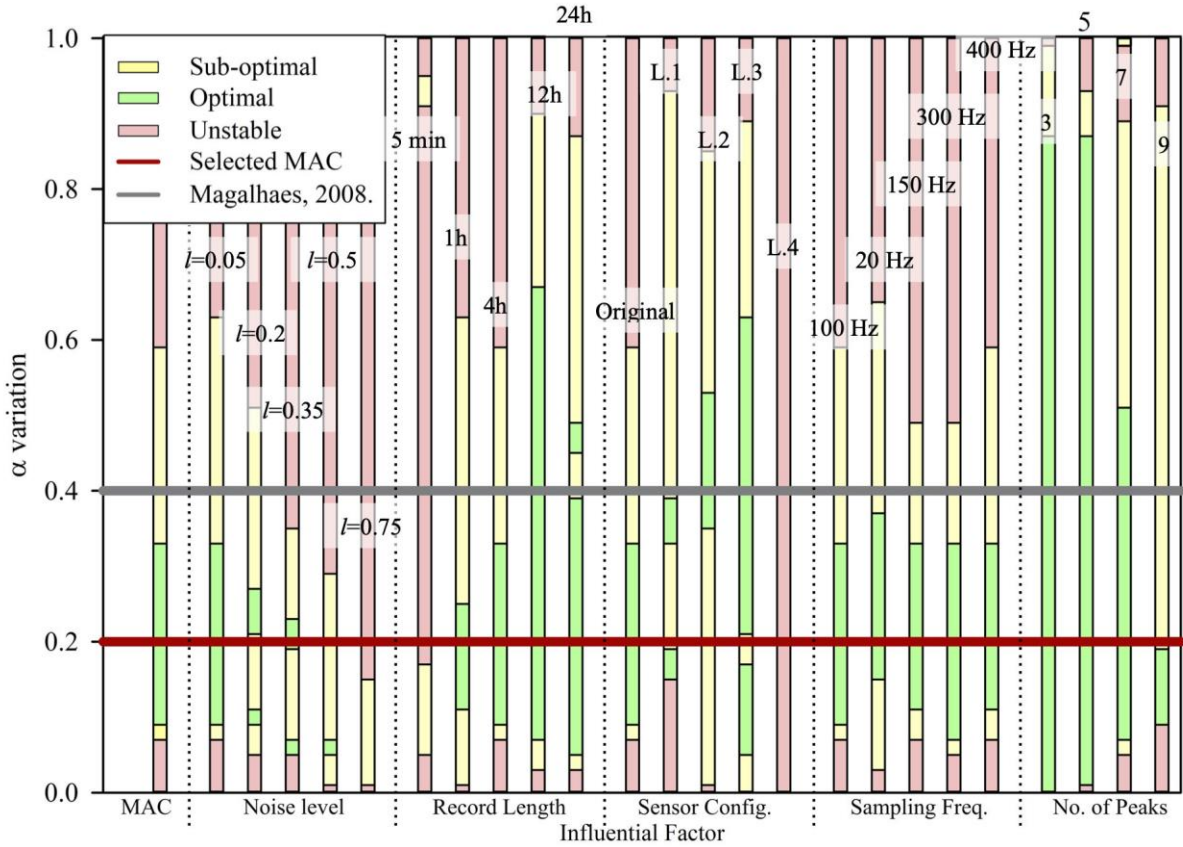


Fig. 3-11. The sub-optimal/optimal ranges derived from sensitivity analysis for each case.

Furthermore, in the rest of this study, the modal domain assessment is activated to verify that the selected peak in the SV spectrum is associated with a physical mode. The verification is made by considering 7 points in the spectrum with a mean MAC of 0.6 or higher. It will ensure gradual MAC variation observed when detecting physical mode shapes.

## 4. METHODOLOGY VALIDATION

### 4.1. Case study 1: Yonghe cable stayed bridge

The acceleration records plotted in Fig. 4-1 in the vertical direction, collected from 03:00 AM to 04:00 AM on January 17, 2008, were used to test and validate the AFDD procedure.

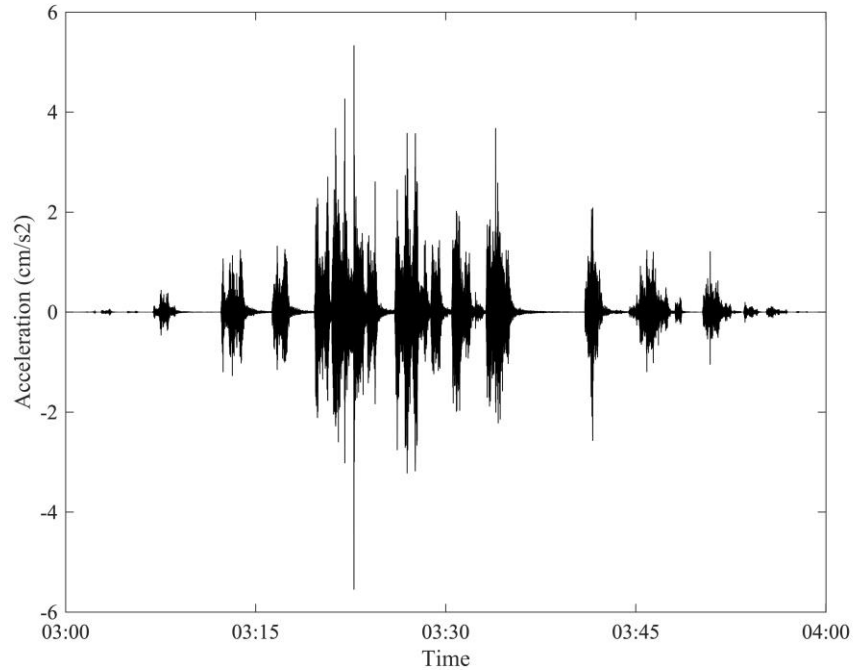


Fig. 4-1. The acceleration recorded by sensor 14 on the cable stayed bridge.

Considering the frequency range of 0-1.3 Hz, the number of desired frequencies was set to 6, as the number of frequencies resulting from the FE modal analysis. Fig. 4-2.a shows the peaks automatically selected in the SV spectrum and the corresponding identified modal frequencies resulting from AFDD analysis.

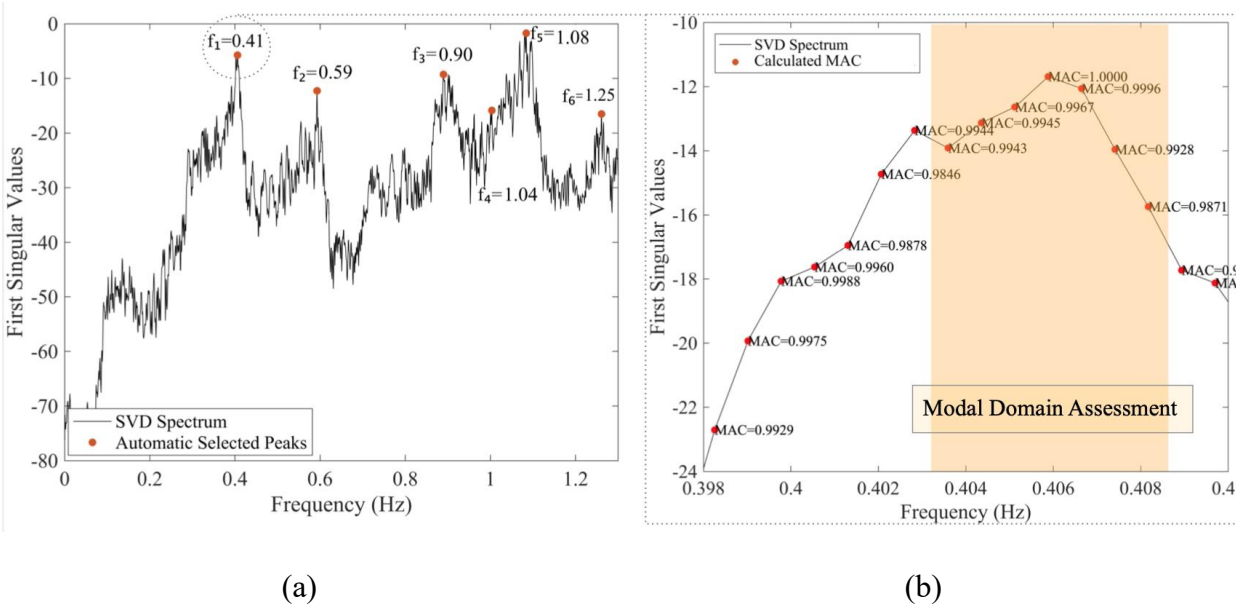


Fig. 4-2. AFDD analysis of the cable-stayed bridge for 1-hour signal: (a) selected peaks in the SV spectrum, and (b) MAC evaluation for the first selected peak and modal domain assessment.

The MAC variation is depicted for the first identified peak with the frequency of 0.41 Hz in Fig. 4-2.b to provide an insight into the modal domain assessment around each peak. It is evident that the MAC mean in this modal domain is much larger than the prescribed threshold. In addition, a wider modal domain could be considered to verify the presence of physical modes. However, this behavior is only limited in detecting vertical modes since their geometry highly differ. The 3D vertical mode shapes obtained from the AFDD are illustrated in Fig. 4-3. The mode shapes were drawn by spline interpolation between the sensor locations.

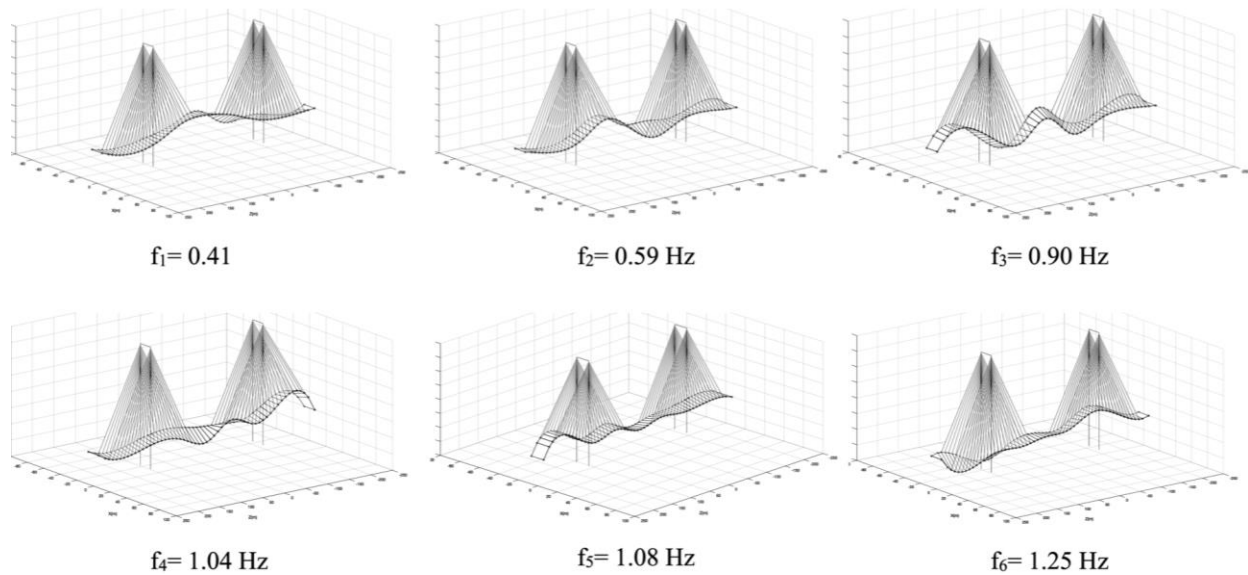


Fig. 4-3. 3D deformed configuration of the Yonghe cable-stayed bridge.

Subsequently, the cov-SSI analysis was performed, interpreting its stabilization diagram to avoid unstable mode identification. Over the task, based on the referenced criteria in the introduction, the time lag was set at 366, and the model order to 120.

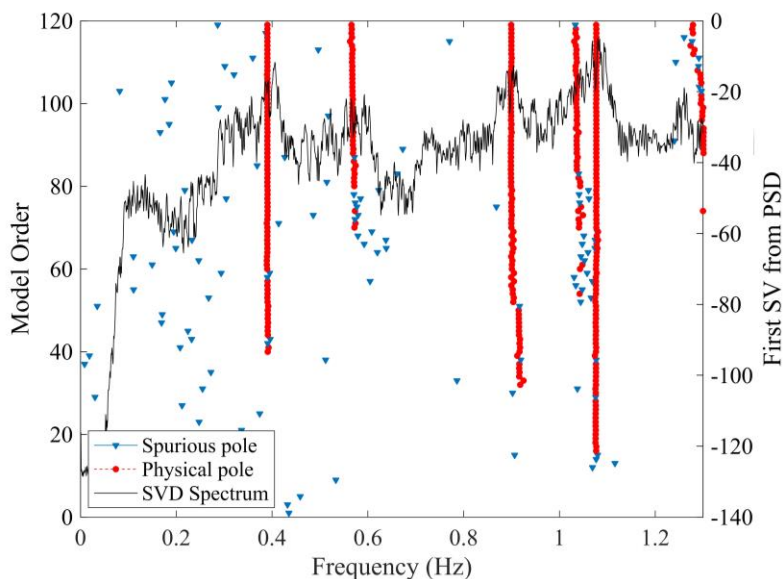


Fig. 4-4. Stabilization diagram for the cov-SSI analysis of the Yonghe cable-stayed bridge for 1-hour record.

Fig. 4-4. presents a stabilization diagram containing spurious and physical poles in which the x-axis and y-axis are frequencies and model order, respectively. A physical mode emerges from an almost vertically aligned set of stable physical poles, and thus, six modes are identified with natural frequencies:  $f_1=0.39$  Hz,  $f_2=0.56$  Hz,  $f_3=0.90$  Hz,  $f_4=1.03$  Hz,  $f_5=1.08$  Hz,  $f_6=1.28$  Hz.

The analysis was repeated for an additional signal recorded from 01:00 am to 12:00 pm on January 17, 2008, using the same parameters described for the 1-hour record. The automatically selected peaks and identified frequencies are presented in Fig. 4-5 and Fig. 4-6.

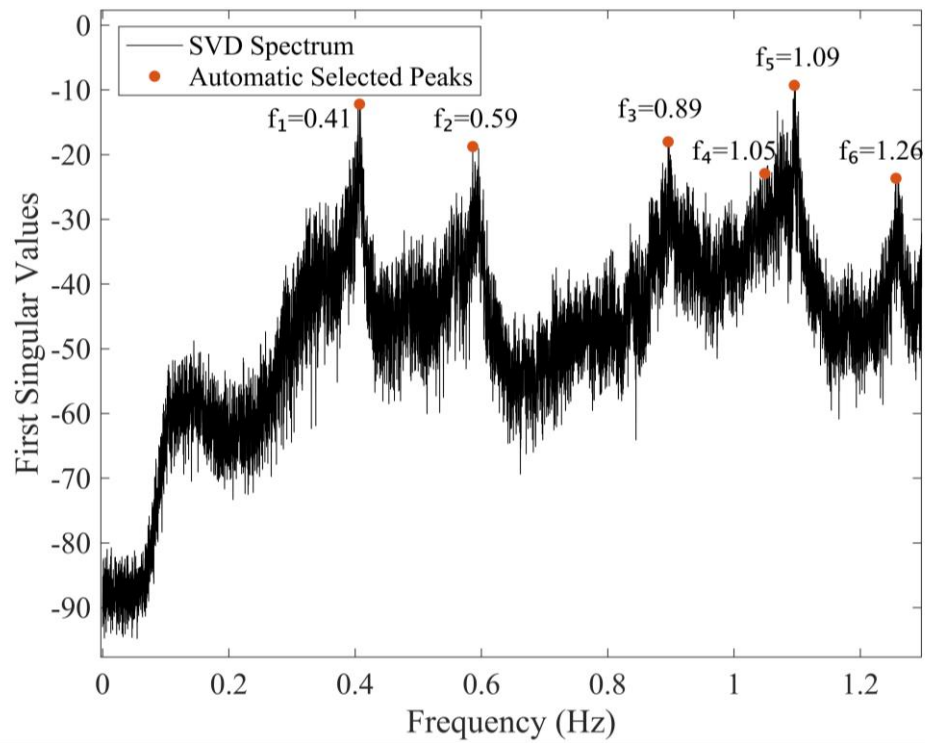


Fig. 4-5. AFDD analysis of the cable-stayed bridge for 12-hour signal

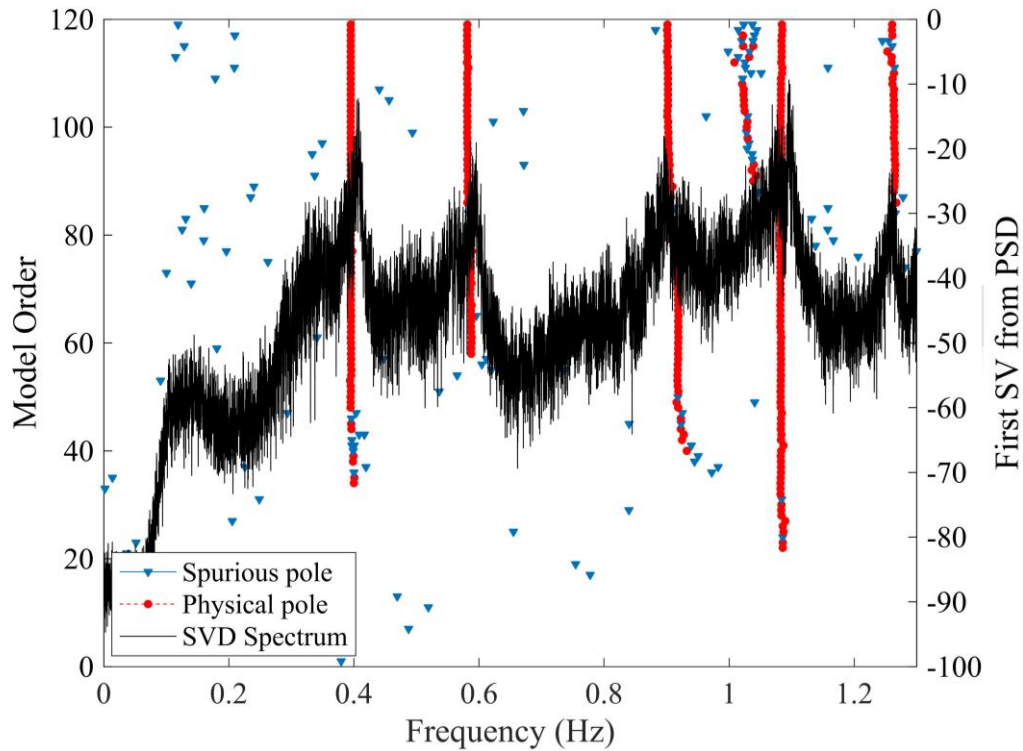


Fig. 4-6. Stabilization diagram for the cov-SSI analysis of the Yonghe cable-stayed bridge for 12-hour record.

Here, since the record length increases, the windows segmentation and the number of points used for the Fast Fourier Transform (FFT) of the input signal to derive PSD is increased proportionally, leading to a high-density SV spectrum. Despite the denser spectrum with higher risks in selecting the spurious peaks, the AFDD performs accurately. Additionally, as indicated in Fig. 4-6, the cov-SSI analysis led to identifying five physical modes with the following frequencies:  $f_1=0.39$  Hz,  $f_2=0.58$  Hz,  $f_3=0.90$  Hz,  $f_6=1.08$  Hz,  $f_7=1.26$  Hz. However, a vague condition rises within the frequency range of 0.95-1.05 Hz, splitting the vertical line formed by physical poles into two branches from the model order of 107. As a result, the mode with 1.02 Hz is selected as the stable one between the two branches since it aligns with the previous physical poles better.

Finally, the traditional FDD was performed.

The comparison of extracted frequencies of vertical mode shapes between the traditional FDD, the cov-SSI, the optimized AFDD, and the FE modal analysis is presented in Table 1.

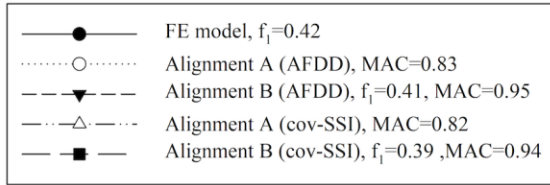
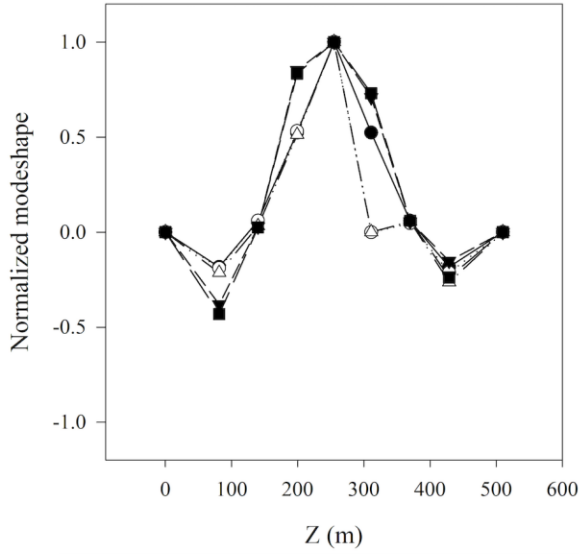
Table 1. Comparison of the Yonghe cable-stayed bridge frequencies.

Method	FE model	FDD, Li et al. (2014)	Cov-SSI (1h)	AFDD (1 h)	Cov-SSI (12 h)	AFDD (12 h)
	0.42	0.42	0.39	0.41	0.39	0.41
	0.59	0.59	0.56	0.59	0.58	0.59
Identified	0.88	0.89	0.90	0.90	0.90	0.89
Frequencies	1.04	1.04	1.03	1.04	1.02	1.05
(Hz)	1.09	1.10	1.08	1.08	1.03 <sup>a</sup>	1.09
	1.21	1.27	1.28	1.25	1.08	1.26
	-	-	-	-	1.26	-

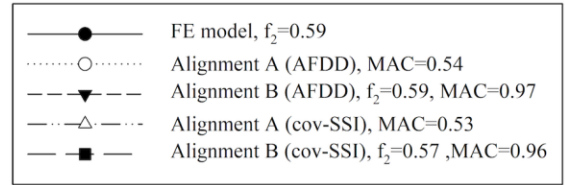
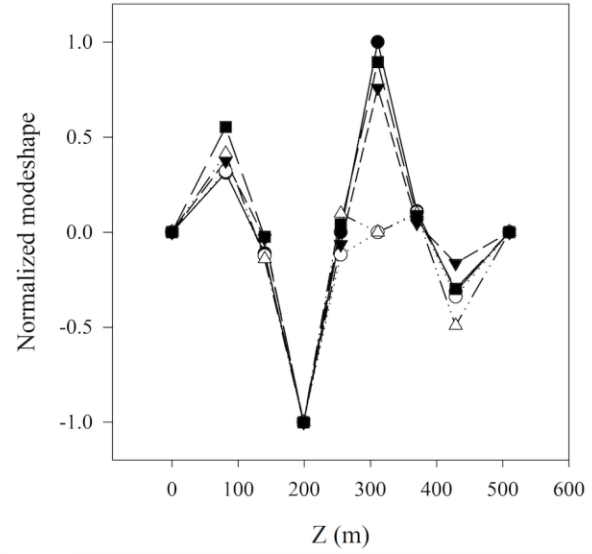
<sup>a</sup>Frequency incorrectly identified.

Within the frequency range of 0-1.3 Hz, all methodologies were able to identify at least six frequencies. Regarding the 1-hour record, the AFDD results exhibited greater proximity to the FE model frequencies in comparison with the results obtained from the cov-SSI approach. In the case of the 12-hour signal, the AFDD also performed better, and the time domain analysis identified an extra mode with a 1.03 Hz frequency.

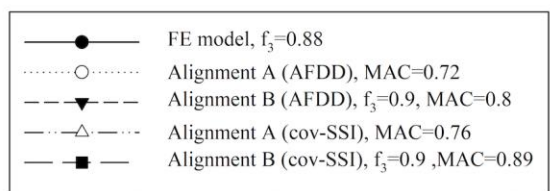
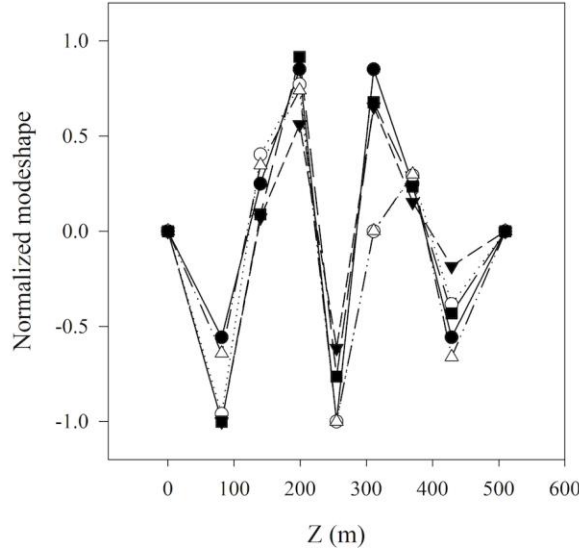
To evaluate the consistency of the mode shapes extracted by the different methods, they were plotted in Fig. 4-7, separating the results for sensor alignments A and B.



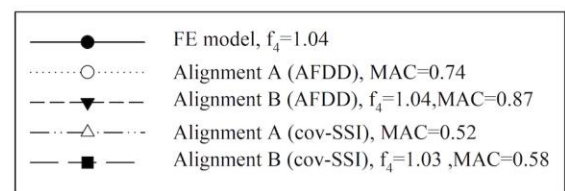
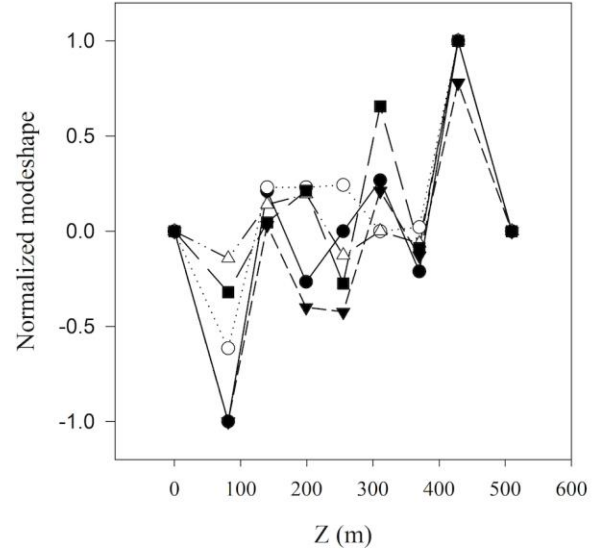
(a)



(b)



(c)



(d)

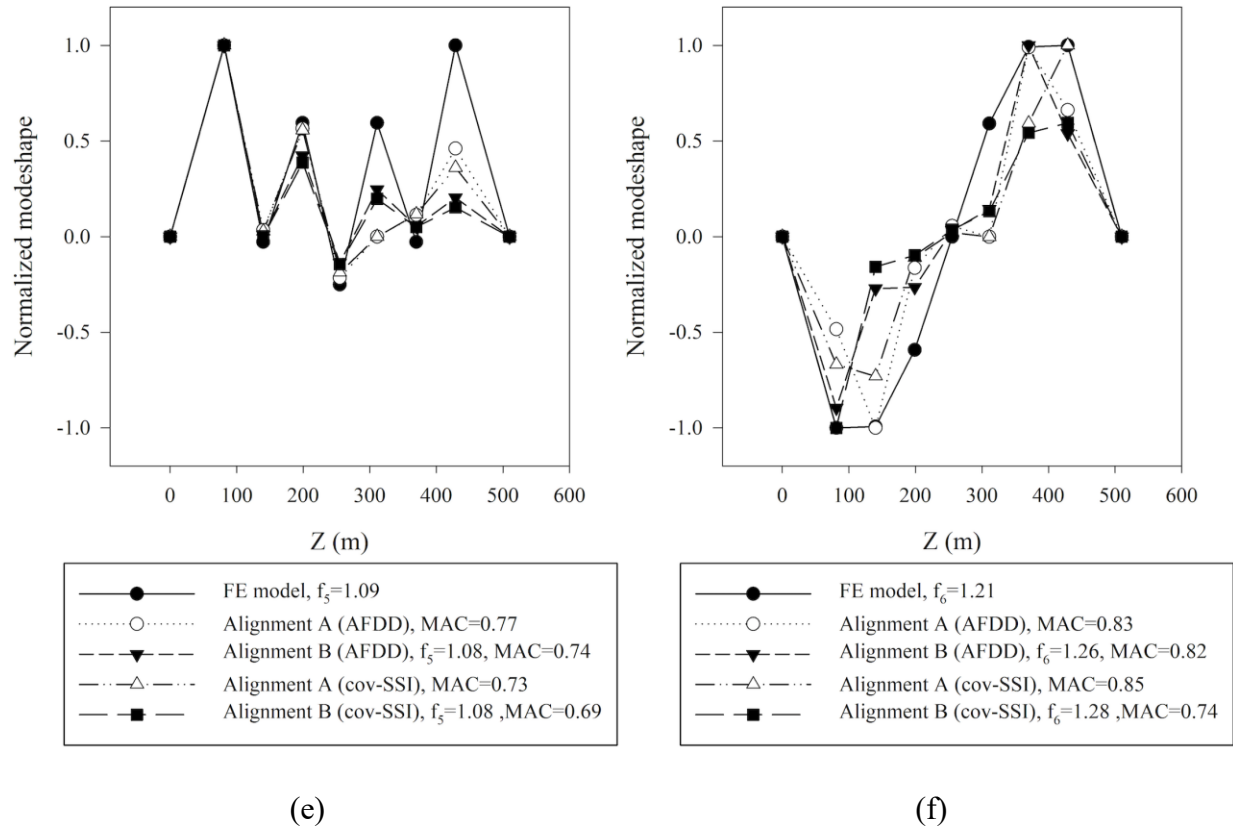
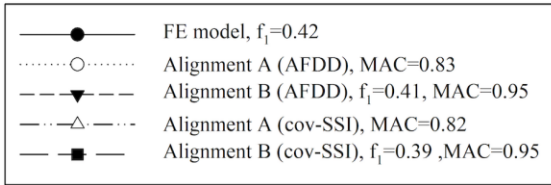
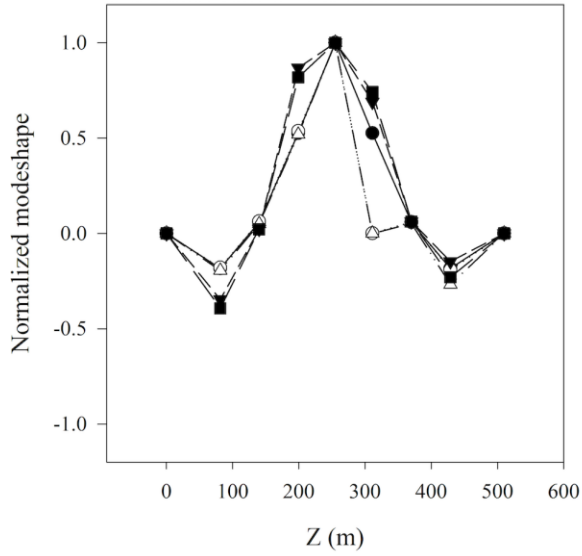


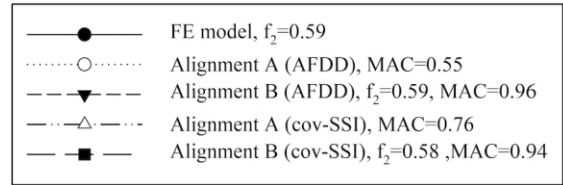
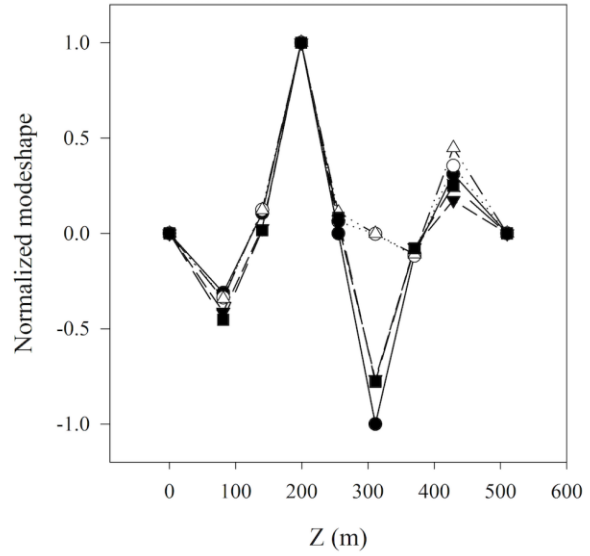
Fig. 4-7. Comparison of derived mode shapes for Yonghe cable-stayed bridges (1 h duration), (a) first mode, (b) second mode, (c) third mode, (d) 4<sup>th</sup> mode, (e) 5<sup>th</sup> mode, (f) 6<sup>th</sup> mode.

The horizontal axis indicates the sensor locations in each plot while the presented modal values have been normalized by their maximum magnitudes. Additionally, the MAC values are computed for each sensor alignment and processing technique, serving as a measure of consistency between the derived modes and their FE counterparts. Notably, larger MAC values characterize the mode shapes from AFDD analysis juxtaposed with cov-SSI estimates, particularly pronounced for the fourth mode at 1.04 Hz frequency. The distortions seen around sensor No.10, located at 350 m, are due to a malfunction visible from the raw data both in the time and frequency domains. On the other hand, differences could be mainly due to the fact that the FE model considers the longitudinal middle axis of the bridge, whereas the sensors are placed on the sides of the deck.

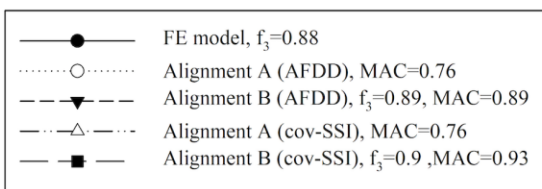
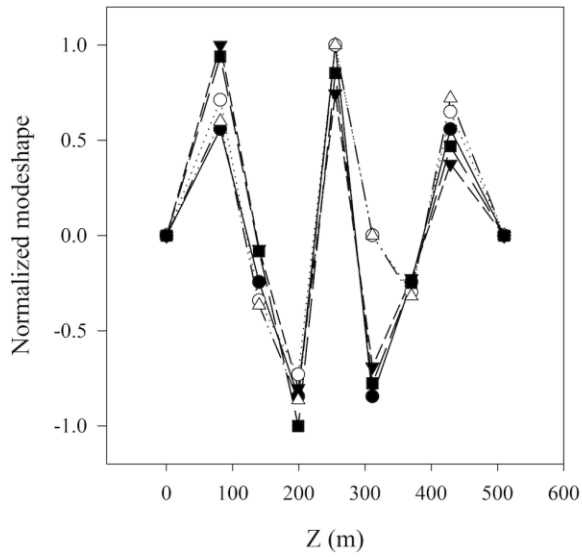
Similar comparison is made for the case of 12-hour input signal.



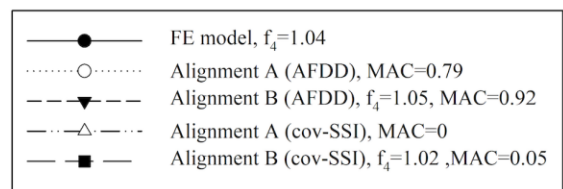
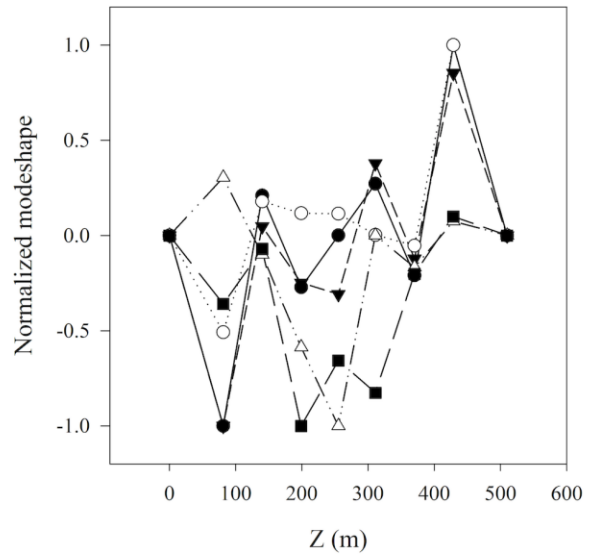
(a)



(b)



(c)



(d)

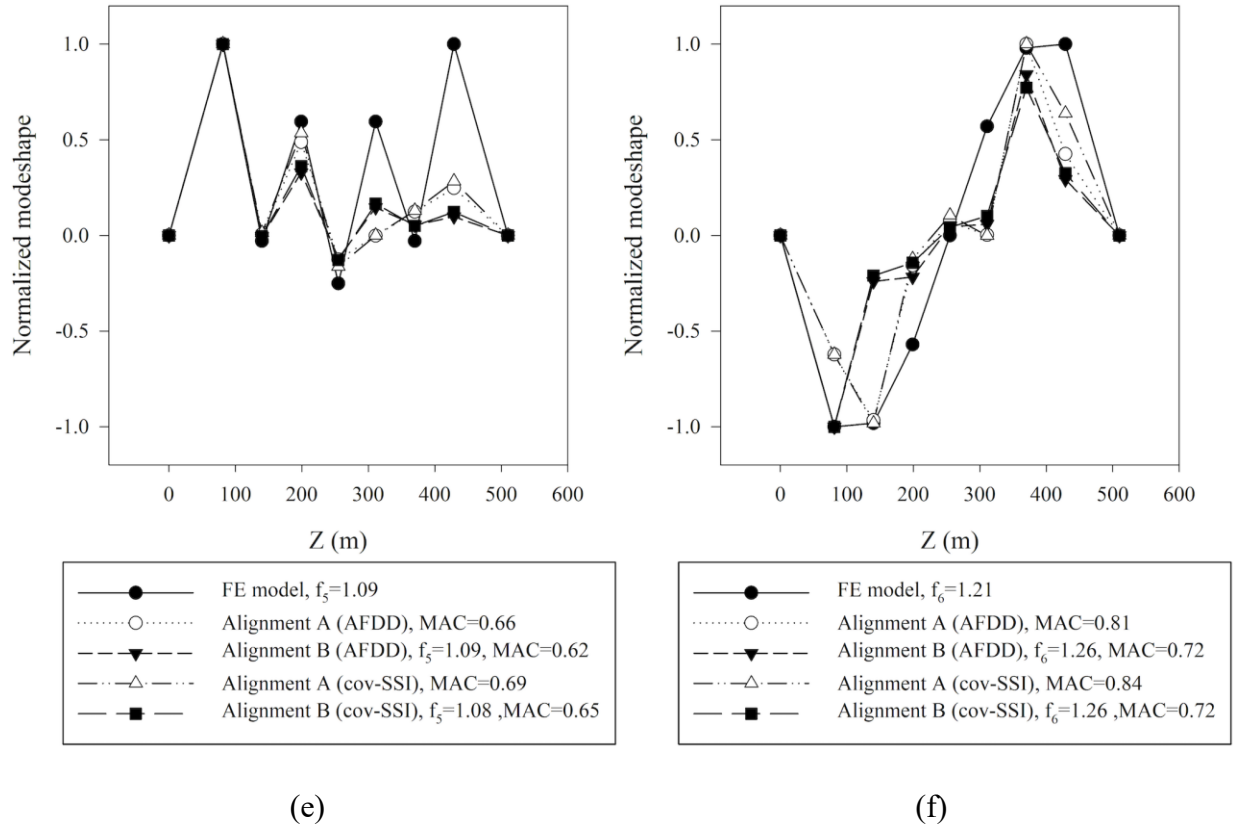


Fig. 4-8. Comparison of derived mode shapes for Yonghe cable-stayed bridges (12 h duration), (a) first mode, (b) second mode, (c) third mode, (d) 4<sup>th</sup> mode, (e) 5<sup>th</sup> mode, (f) 6<sup>th</sup> mode.

Fig. 4-8.d highlight the limitation exist in the cov-SSI in which a spurious mode is selected as stable one. In overall, increasing the length of input signal result in higher accuracy in the estimated mode shapes by AFDD.

This application demonstrates the effectiveness of the optimized AFDD method, yielding highly accurate outcomes. Moreover, the utilization of this method mitigated selecting spurious peaks when identifying vertical modes of vibration, in stark contrast to the cov-SSI approach.

#### 4.2. Case study 2: PolyU footbridge

The PolyU footbridge is an irregular structure with butterfly-shaped steel tube arches located at Hong Kong Polytechnic University. It consists of primary and two-side concrete spans

with a length of 84.24 m and 64.26 m, respectively, supported by hangers connected to two inclined arches.



Fig. 4-9. PolyU footbridge located in the Hong Kong Polytechnic University.

Throughout the construction phase, an inventive SHM system was incorporated into the footbridge's framework and commenced data acquisition on September 28, 2019. The system includes a combination of three-axial and uniaxial accelerometers, spatially distributed optical sensors, FBG sensors, and a global navigation system. The accelerometers, with a sampling frequency of 50 Hz, are mounted on the sides of the deck along two alignments, as illustrated in Fig. 4-10. The sensors placed along alignment B are three-axial, whereas those on alignment A can record only vertical accelerations.

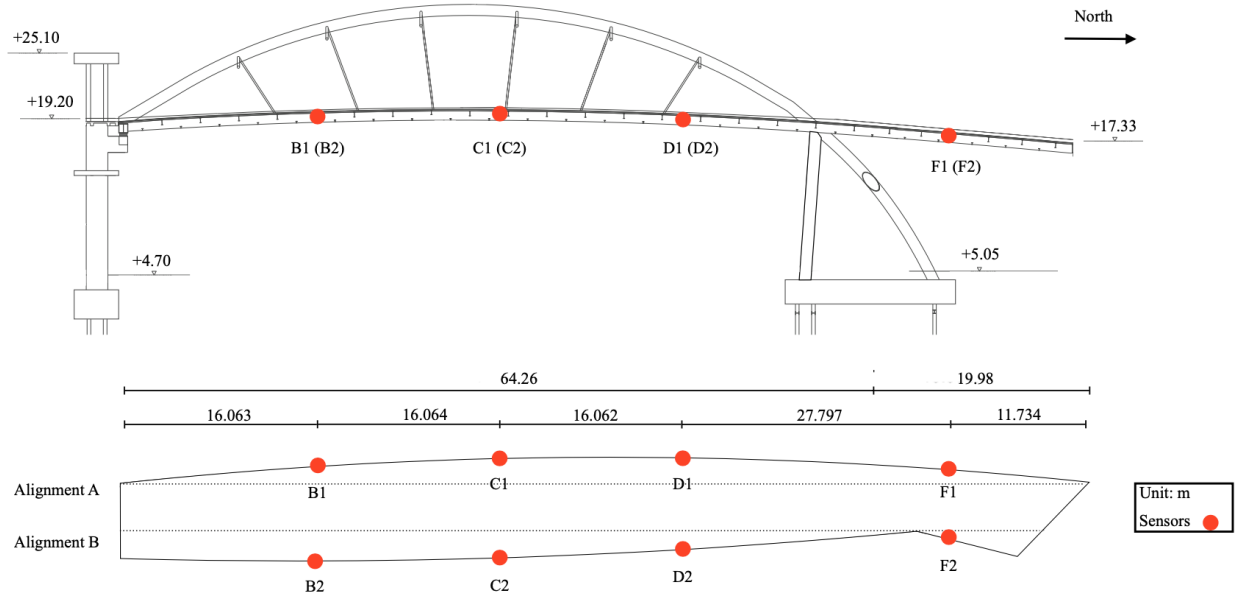


Fig. 4-10. The SHM layout mounted on the PolyU footbridge.

A 3D Finite Element model of 8,785 elements was developed to simulate the dynamics of the bridge and calibrated according to the modal properties acquired from the SSI method. The FE analysis revealed the presence of combined vertical and torsional mode shapes (Xia et al. 2021). The modal properties obtained through the FE modal analysis and SSI were used to compare the results of the current study.

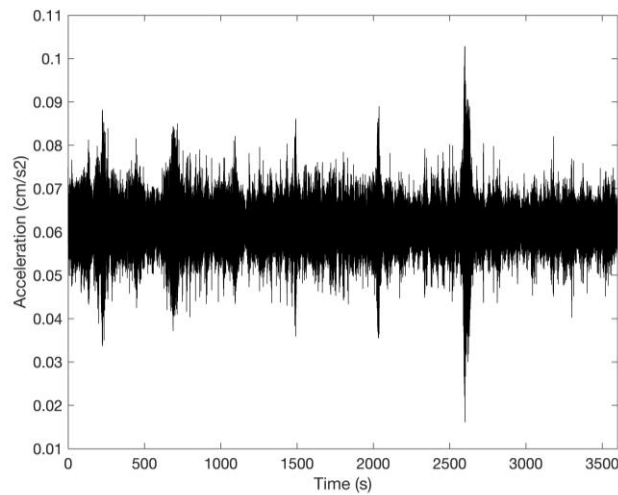


Fig. 4-11. Vertical acceleration recorded by sensor B2 on the PolyU footbridge.

The vibration recorded from 00:00 AM to 01:00 AM, November 1, 2019, is used to extract the modal properties as illustrated in Fig. 4-11.

For the AFDD analysis, the frequency range of interest was fixed to 0-3.2 Hz and the number of desired frequencies to 6. Fig. 4-12 presents six peaks automatically detected by the AFDD procedure and their corresponding frequency. An intriguing observation is the identification of modes with frequencies of 1.67 Hz and 1.8 Hz, a distinctive capability not conventionally made using traditional FDD techniques.

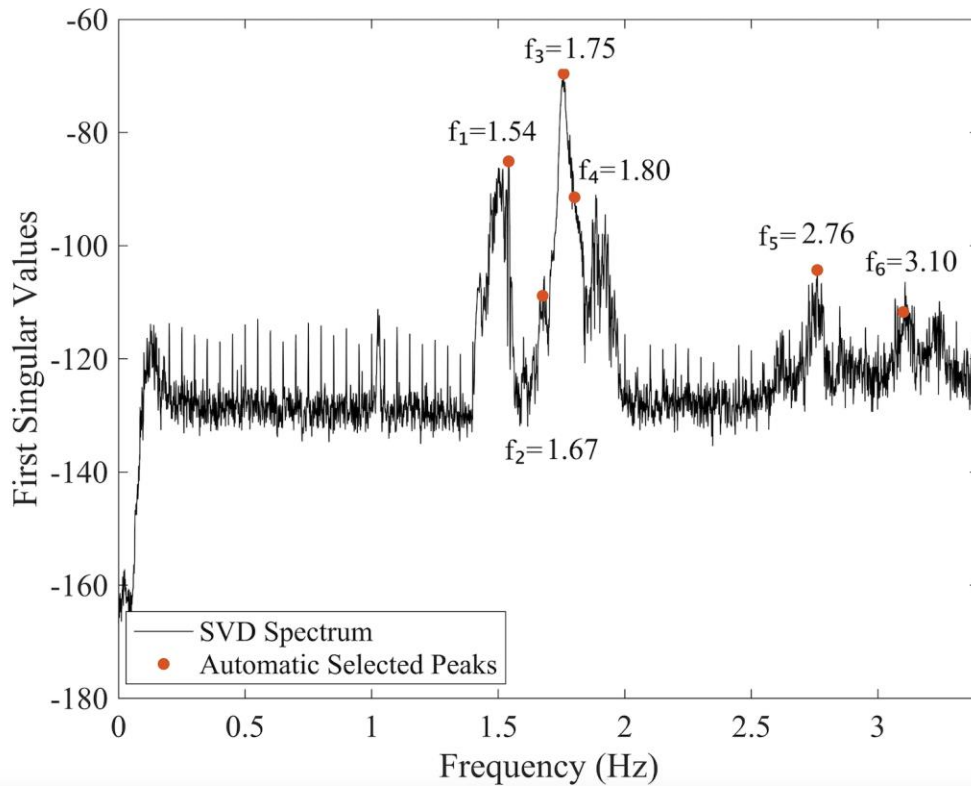


Fig. 4-12. The automatically selected peaks in the SV spectrum by AFDD analysis for PolyU.

The resultant mode shapes are illustrated in Fig. 4-13.

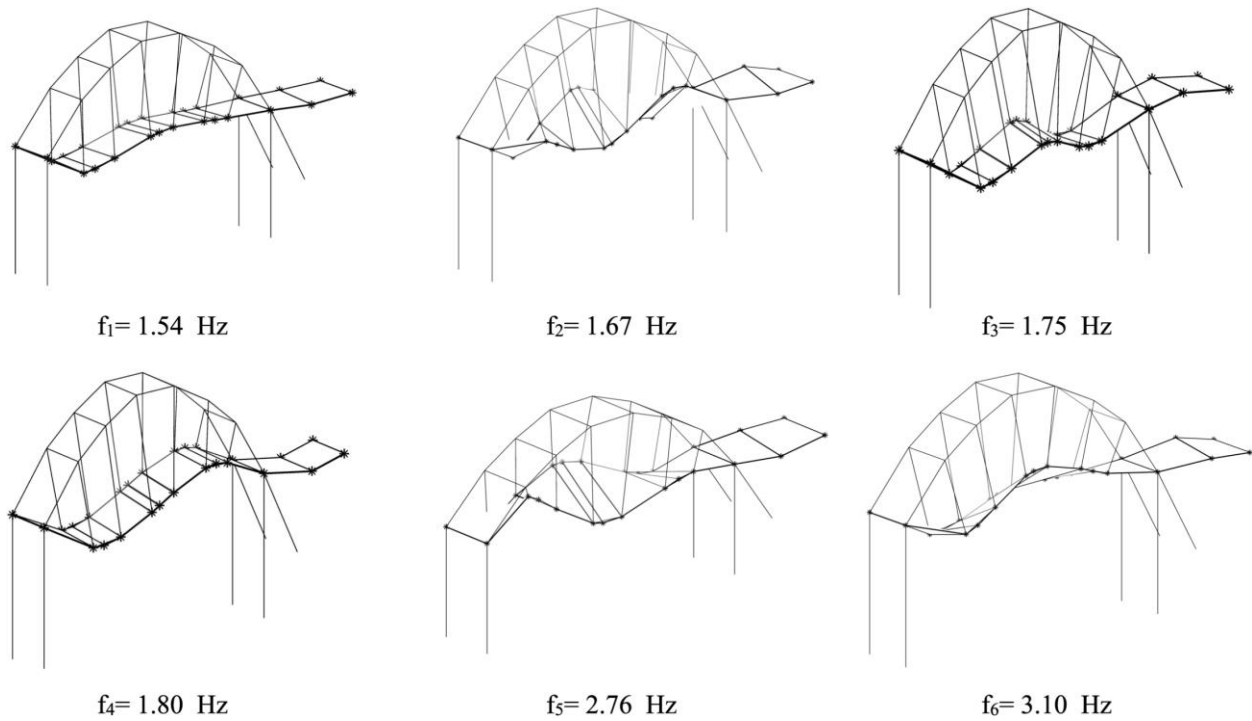


Fig. 4-13. 3D deformed configuration of the PolyU footbridge.

In the cov-SSI analysis, the system order was set equal to 100 following the work done by Xia (Xia et al. 2021). Moreover, the time lag is set equal to 65 since the fundamental frequency is 1.16 Hz. The stabilization diagram is plotted in Fig. 4-14, which shows the presence of 5 stable modes with the following natural frequencies:  $f_1=1.5$  Hz,  $f_2=1.75$  Hz,  $f_3=1.78$  Hz,  $f_4=1.91$  Hz,  $f_5=2.75$  Hz. In addition, an unstable mode at 1.85 Hz can be observed, vanishing from model order 89.

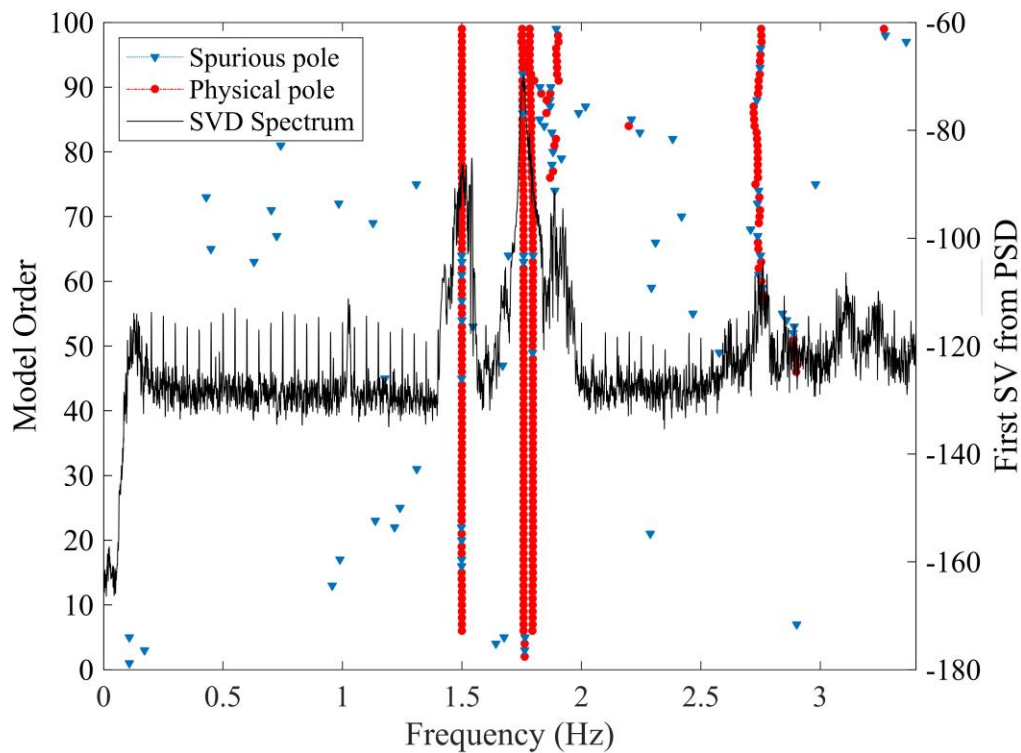


Fig. 4-14. The resultant stabilization diagram for the PolyU footbridge.

Table 2 highlights the extracted frequencies obtained from AFDD and cov-SSI, addressing new findings compared to the study of 2019.

The symmetry and orientation of each mode shape are also clarified based on the 3D deformed geometry. The initial study conducted in 2019 unveiled the presence of four dynamic modes within the frequency range of 1.8 to 3.10 Hz. However, the current analysis increases the number of identified modes to 5 by performing the cov-SSI analysis, discarding the unstable ones. Nevertheless, the cov-SSI encountered limitations in capturing two modes: 1) The torsional mode with the frequency of 3.1 obtained from SSI (2020) and AFDD. 2) The torsional mode at the frequency of 1.67 Hz, taken from AFDD analysis. Furthermore, the optimized AFDD detects six modes, and the deck torsional one with a frequency of 1.94 Hz (from SSI analysis) is missing. The geometrical similarity between the torsional mode and the vertical one with a frequency of 1.8 Hz

prevents the identification of the torsional one. Indeed, the MAC calculated between them is 0.74. In general, a low spatial resolution of instrumented sensors can arise this issue, and a compromise between the cost of a monitoring campaign and outcome accuracy is inevitable.

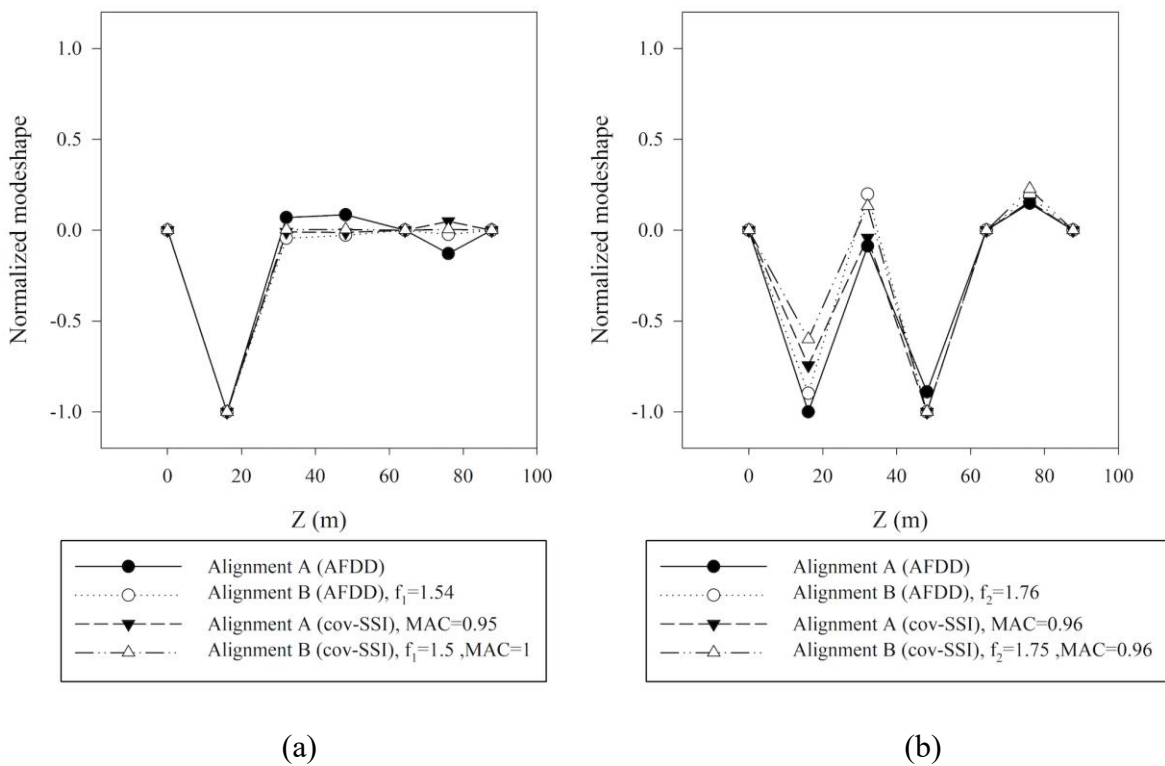
Table 2. Comparison of the Poly-U footbridge frequencies.

Method	FE	SSI (2020)	Description	AFDD	Description	Cov- SSI
Identified Frequencies (Hz)	1.80	1.88	Deck vertical	1.54	Combination of vertical and lateral on the half of the bridge	1.50
	2.04	1.94	Deck Torsional	1.67	Deck Torsional, symmetrical in x- dir, skew sym. In y-dir	–
	2.81	2.63	In-plane bending	1.75	Combination of vertical and lateral and torsional	1.75
	2.97	3.10	Deck Torsion	1.80	Vertical, skew symmetrical	1.78
				–	Deck Torsional	1.91
				2.76	Transversal and torsional	2.75
				3.10	Torsional	–

The AFDD analysis revealed the presence of three new modes below 1.8 Hz, which was the first frequency according to the study in 2020. It was also confirmed through the cov-SSI analysis, which identified two frequencies below 1.8 Hz. Since the acceleration records used here

differ from those in the previous work, the newly identified modes might be associated with an additional vibration source. However, this would require further investigation, which is beyond the scope of the current study.

The mode shapes obtained through the AFDD and cov-SSI methods, sharing similar natural frequencies, for alignments A and B are plotted in Fig. 4-15. In the figure, the x-axis corresponds to sensor locations, and the y-axis presents the modal values normalized by the highest magnitude. In this case, it was impossible to compare the results to the FE model for confidentiality reasons.



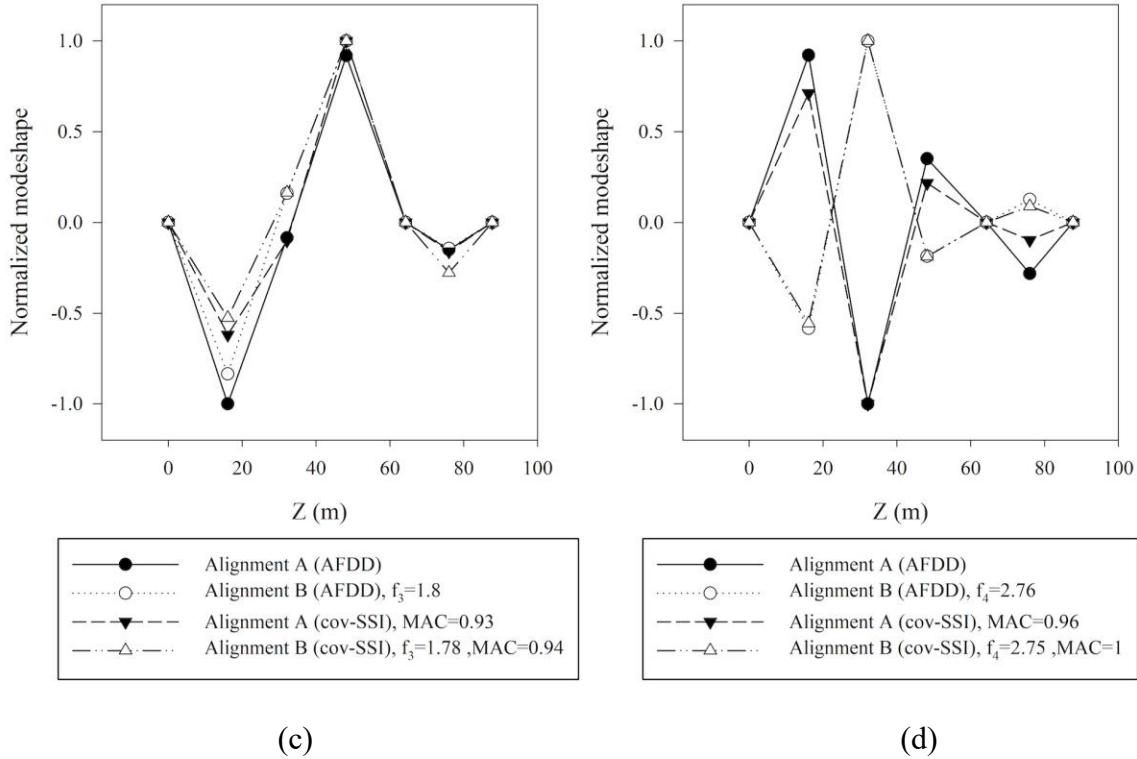


Fig. 4-15. Comparison of extracted mode shapes from PolyU footbridge, (a) first mode, (b) second mode, (c) third mode, (d) fourth mode.

Therefore, the MAC was calculated only between the modal vectors obtained via AFDD and cov-SSI. The high consistency observed for the modes with a natural frequency below 1.8 Hz further indicates they are not associated with noise contamination in the input signal. Overall, the highest consistency is observed for the mode with a natural frequency of 2.76 Hz. The plots highlight the complexity of the modal geometries, making the modal identification task challenging.

It holds significant importance to mention identifying torsional modes using the optimized AFDD involves two primary aspects. First, the modal domain, where a gradual change of MAC occurs, is narrower for torsional modes. In other words, in the automated peak picking algorithm, there is a rapid transition in MAC from 0.2 to 1 around a peak associated with a torsional mode in

contrast with a vertical one seen in Fig. 4-2 b. Therefore, the method demands flexibility in setting the threshold regarding the number of SV points and MAC mean in the modal domain assessment. This flexibility is pertinent when confronting case studies with torsional and akin dynamic modes. To this end, a narrow modal domain with seven SV points and MAC mean of 0.6 was prescribed in the methodology to prevent misidentifying a torsional mode as non-physical one. Secondly, identifying combined mode shapes might be intricate because of the similarity between their geometries. It requires optimal sensing strategies and spatial resolution to ensure capturing them.

### 4.3. Case study 3: Moletta tower in Circo Massimo

In order to assess the performance of the AFDD procedure across diverse structural contexts, the Moletta Tower is selected as the third case study. It is a medieval tower and part of the Circus Maximus archaeological site in Rome, Italy.

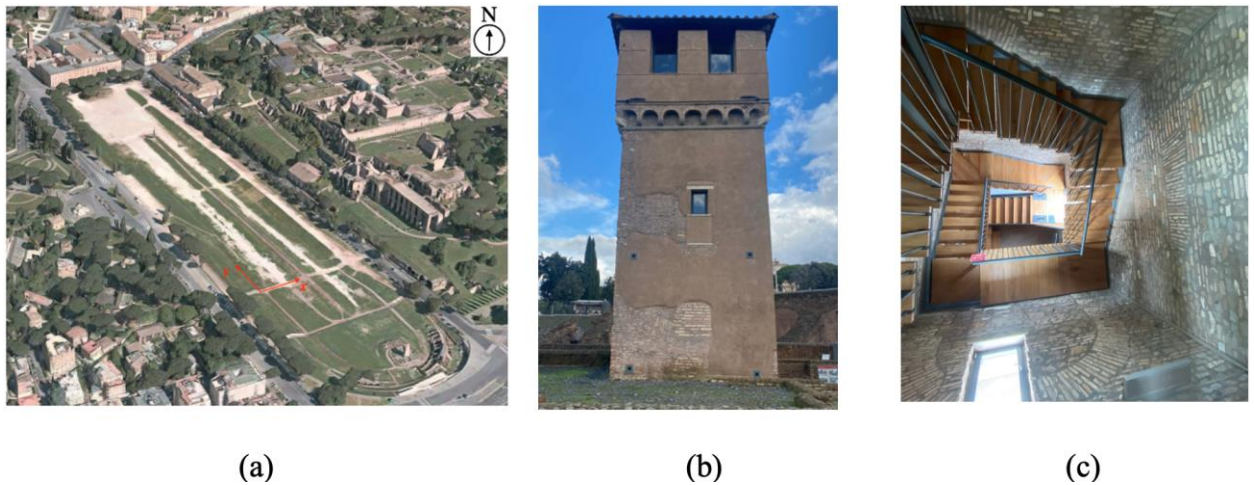


Fig. 4-16. (a) The general view of Maximus circus, (b) Moletta tower, (c) spiral stair case.

The Circus Maximus was built in the first half of the sixth century BC and hosted ancient Roman chariot-racing tournaments. The original track level is buried under 9 m of soil, creating a complex soil-structure interaction.

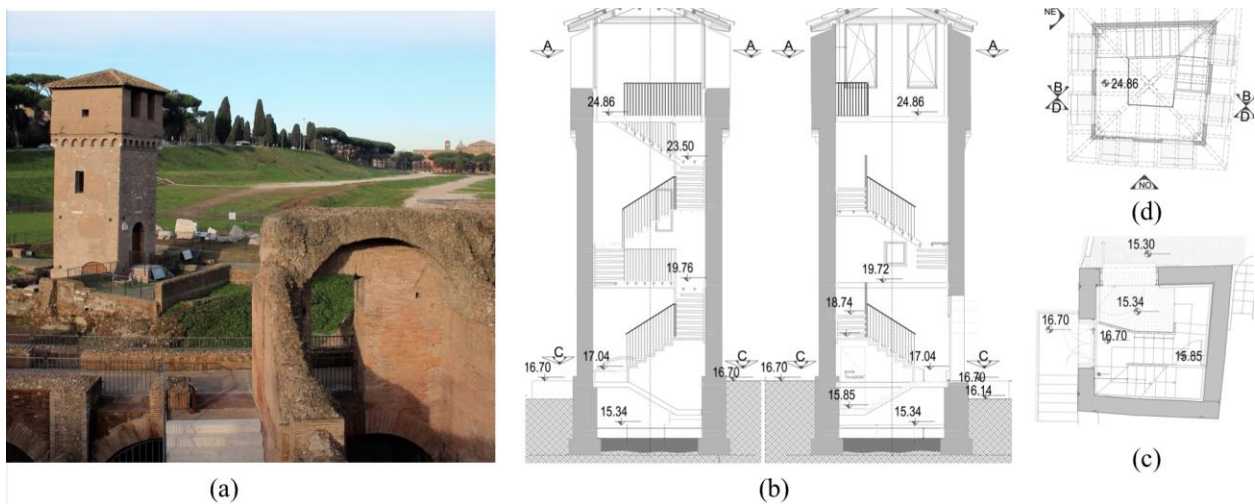


Fig. 4-17. (a) Moletta tower (b) side view of tower. (c) Section C-C. (d) Section A-A.

Nowadays, the venue hosts concerts and entertaining events. For instance, the Rolling Stones concert in 2014 had an estimated attendance of over 70,000 people. Therefore, it is essential to monitor the site and evaluate the impact of anthropic vibrations on the ancient structures. The Moletta Tower is located on the southeast side of the Circus Maximus, as shown in aerial shot of Fig. 4-16.a. In this figure, the Circus's primary axis is denoted as the y-direction, whereas the x-direction aligns orthogonal to it. The structure underwent retrofitting through steel rings and rods, spiral stairs connected to the external walls, and reinforcing its foundations in 2013. Fig. 4-17. displays its irregular plan with non-symmetrical dimensions which induce a complicated dynamic behavior. The tower was monitored by instrumenting Wi-Fi tri-axial accelerometers at various elevations, as shown in Fig. 4-18.

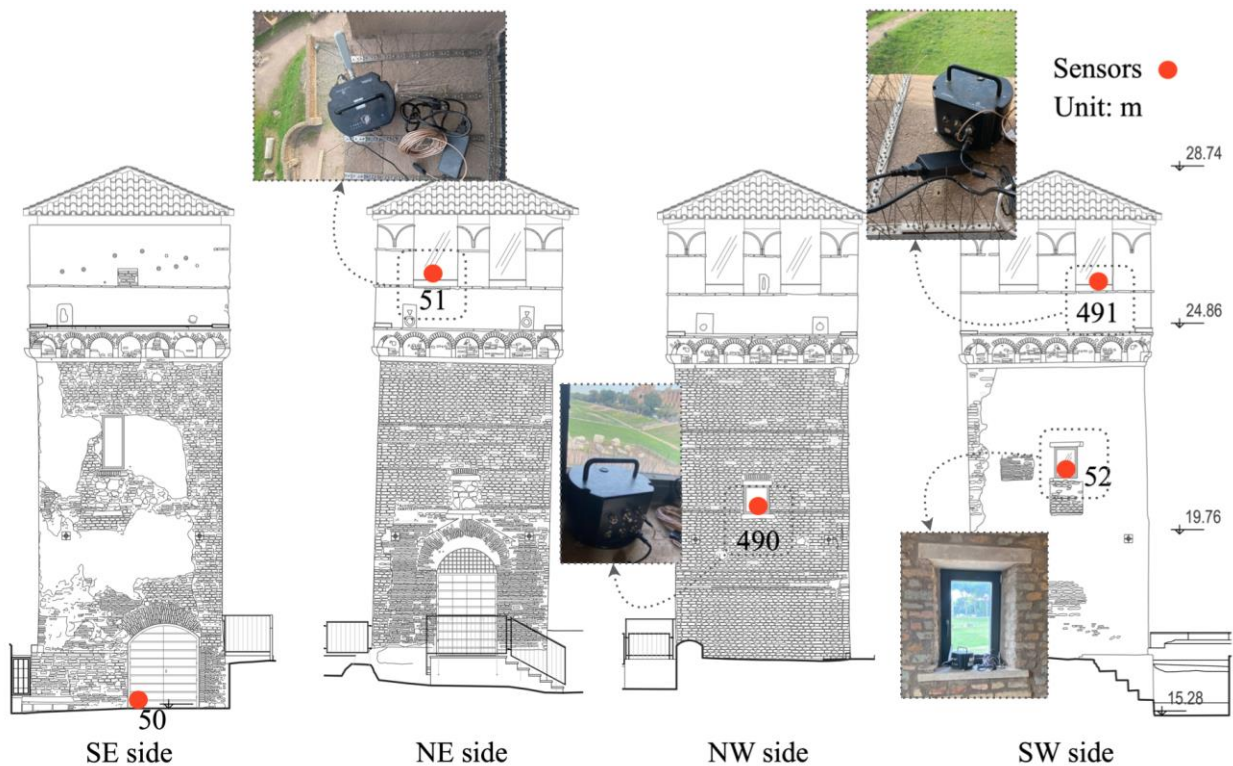
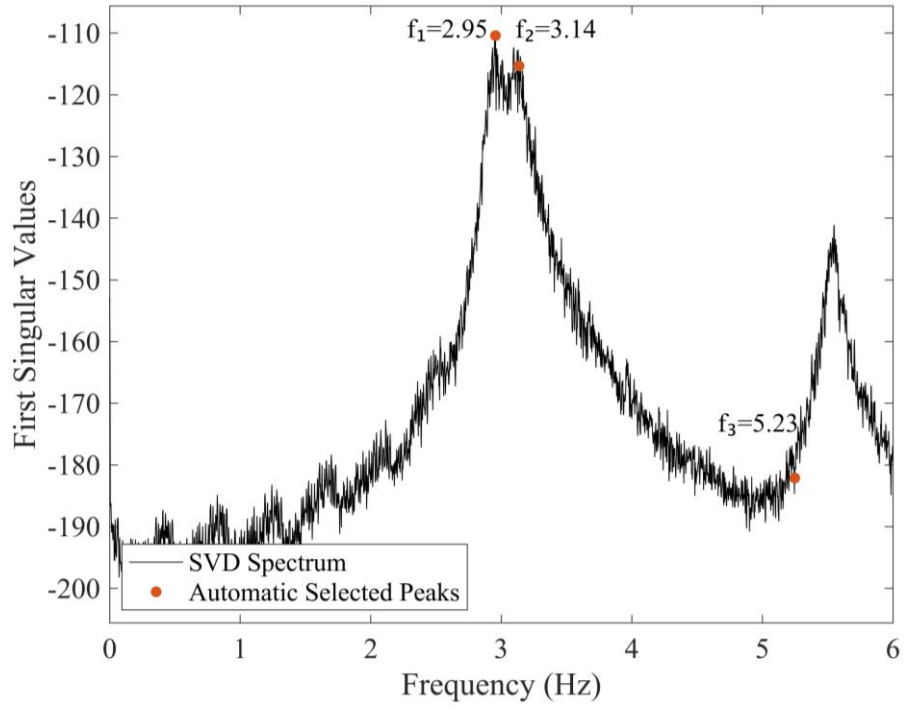
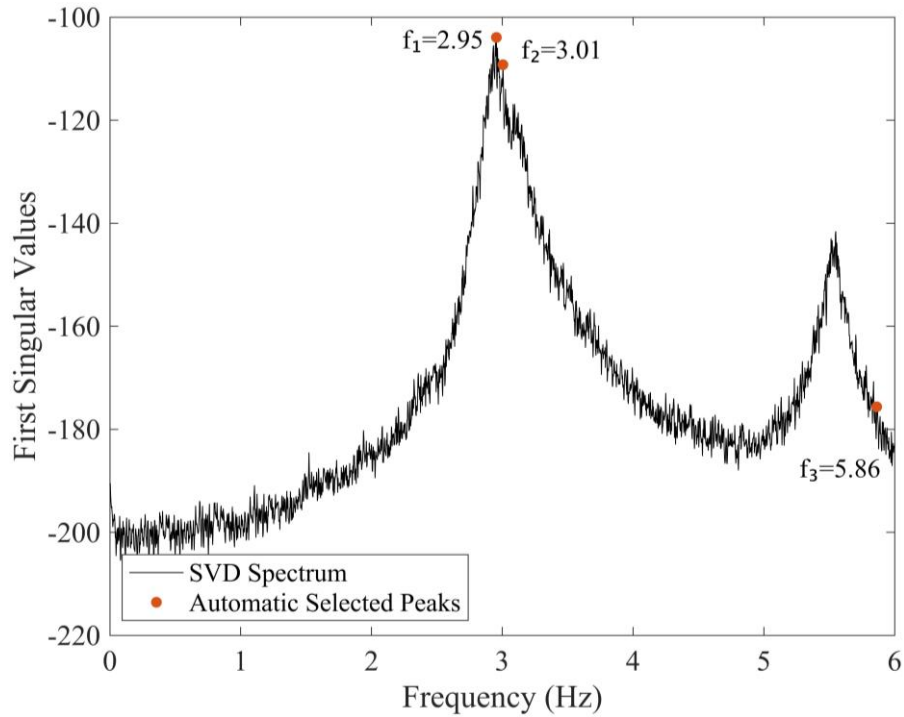


Fig. 4-18. Sensor placement on the Moletta tower.



(a)



(b)

Fig. 4-19. SV spectra and automatically selected frequencies by the AFDD algorithm in (a) x-direction and (b) y-direction.

The acceleration records acquired on October 21, 2022, from 9:15 AM to 10:45 AM UTC were used as input. For the AFDD analysis, the frequency range is fixed between 0 and 6 Hz, and the desired number of mode shapes is set to 3 for all directions.

Fig. 4-19. presents the automatically selected peaks and their corresponding frequencies in the SVD spectrum. Three dynamic modes are identified for both axes. Notably, the AFDD analysis uncovers a mode with a frequency of 3.01 Hz in the y-direction, which is unattainable using the traditional FDD. However, the algorithm doesn't accurately pinpoint the third peak with a frequency of 5.55 Hz. On the x-axis, the third recognized mode is at 5.23 Hz. Further analysis reveals that the SV point at 5.55 Hz is filtered out when selecting the second mode with a frequency of 3.13 Hz since the MAC between the two is equal to 0.57. In the y-direction, an analogous situation occurs. The third selected mode has a frequency equal to 5.86 Hz. The mode at 5.55 Hz is discarded because its MAC with the second identified mode ( $f=3.01$  Hz) is 0.71.

Fig. 4-20. illustrates the 3D mode shapes from AFDD analysis. The top view highlights the rotation of the tower in the modes with frequencies 2.95 Hz and 3.01 Hz, which could be due to the spiral stairs added in the 2013 renovation.

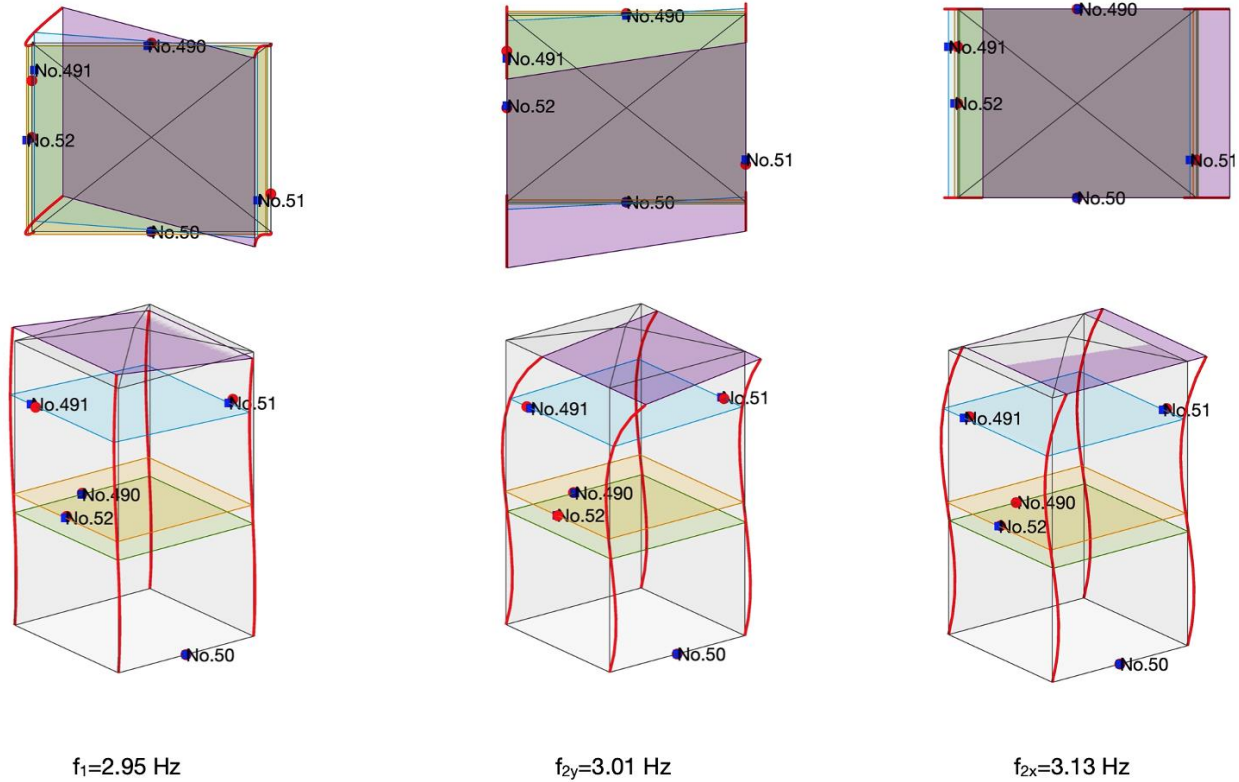
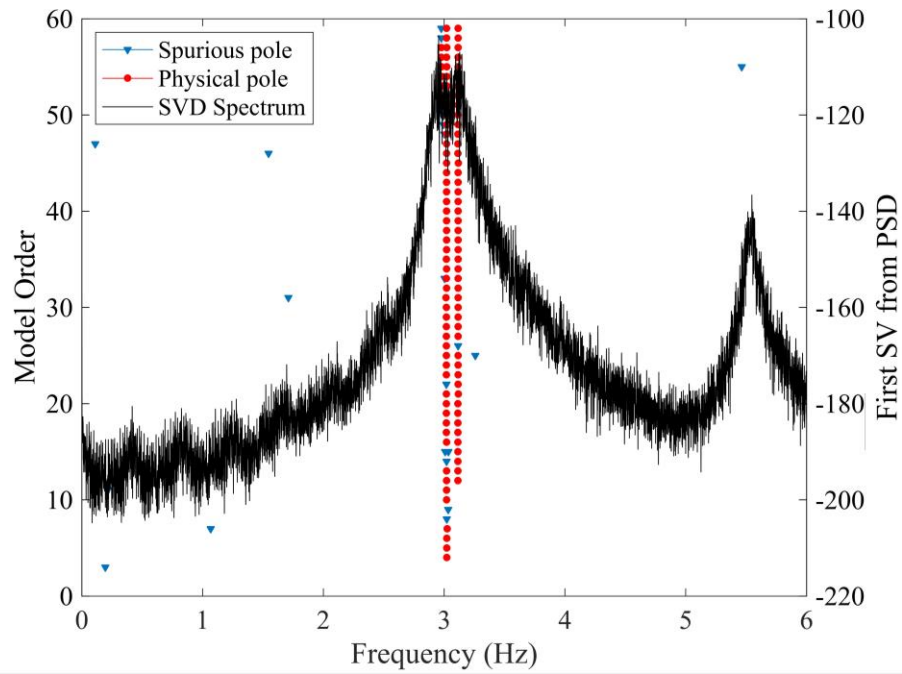
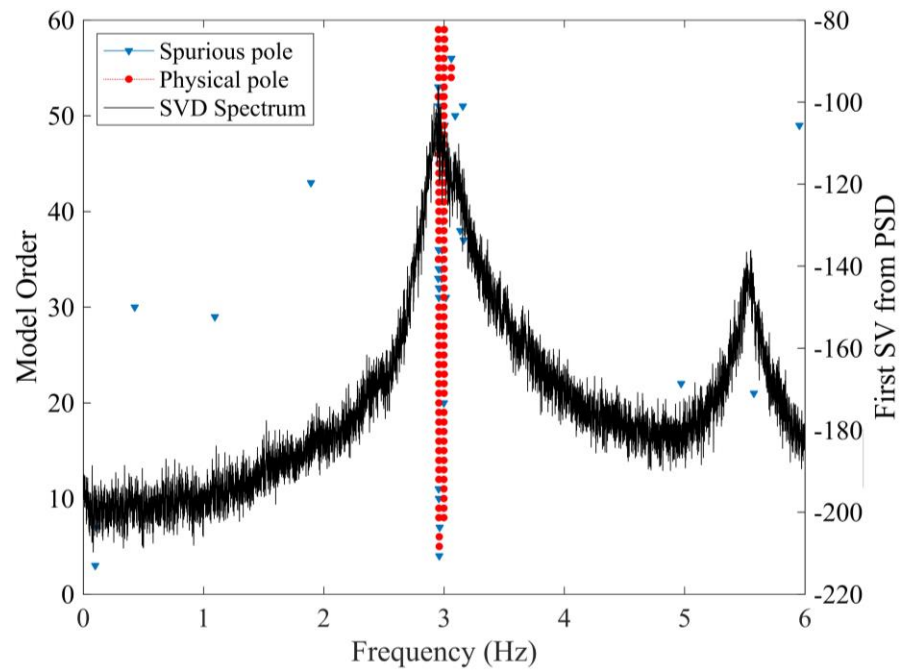


Fig. 4-20. Mode shapes of the Moletta Tower.

For the cov-SSI analysis, a model order of 60 is calculated, and the time lag is 125. The resulting stabilization diagrams for the x and y directions are presented in Fig. 4-21. As depicted in Fig. 4-21. a, three identified peaks with frequencies of 2.97 Hz, 3.02 Hz, and 3.11 Hz, from which the first one is denoted unstable. Similarly, Fig. 4-21.b delineates three identified modes at 2.95Hz, 3Hz, and 3.06 Hz, whereas the third one is unstable. Thus, only two modes exhibit stability for each direction, with no stable pole found beyond 3.3 Hz. It highlights the limitation encountered in using cov-SSI since it doesn't identify the mode resonating at the frequency of 5.55 Hz.



(a)



(b)

Fig. 4-21. Obtained stabilization diagrams for Moletta tower. (a) x-direction, (b) y-direction.

The extracted modal properties are summarized in Table 3 and compared to the study carried on by Puzzilli (Puzzilli et al. 2021). A reduction in frequency estimates can be noticed, which might indicate the dynamics of the structure have changed and stiffness reduced.

Table 3. Comparison of the Moletta Tower frequencies.

Method	FDD, Puzzilli et al.		Manual FDD		AFDD		Cov-SSI	
	(2021)		(2023)		(2023)		(2023)	
Direction	x	y	x	y	x	y	x	y
Identified	3.25	3.00	2.95	2.95	2.95	2.95	3.02	2.95
Frequencies	5.80	5.80	3.13	3.13	3.14	3.01	3.11	3
(Hz)	-		5.55	5.55	5.23	5.86	-	

Despite the AFDD performing better than the cov-SSI, both methodologies provided inaccurate results for third mode. Given the torsional behavior of the structure, a denser sensor layout with two or more sensors on the same level could exhibit better results.

## 5. DEVELOPMENT OF SOFTWARE INTERFACE

In collaboration with Lunitek, an user-friendly software has been developed for OMA analysis of various infrastructures. The primary objectives in designing the interface were:

1. Intuitiveness: Ensuring that users, even those without any expertise in the OMA field, can easily navigate and use the application, particularly the Advanced Frequency Domain Decomposition (AFDD) methodology.
2. Functionality: Displaying results in a clear and informative manner, including graphical representations of AFDD analysis and its outcomes.
3. Customizability: Allowing users to customize the algorithm's settings and parameters to their specific needs.

The interface was developed in the Python environment, a versatile and widely adopted programming language for scientific and engineering applications. PyQt6, a set of Python bindings for the Qt application framework, was chosen for creating the graphical user interface due to its rich set of features and cross-platform compatibility. The software is planned for release on both Mac and Windows operating systems.

The user interface comprises several key elements, including:

- Sensor setup
- Real-time sensor monitoring
- Signal preprocessing
- General analysis
- OMA Covariance-SSI
- OMA Frequency Domain Decomposition (FDD)
- OMA Advanced Frequency Domain Decomposition (AFDD)

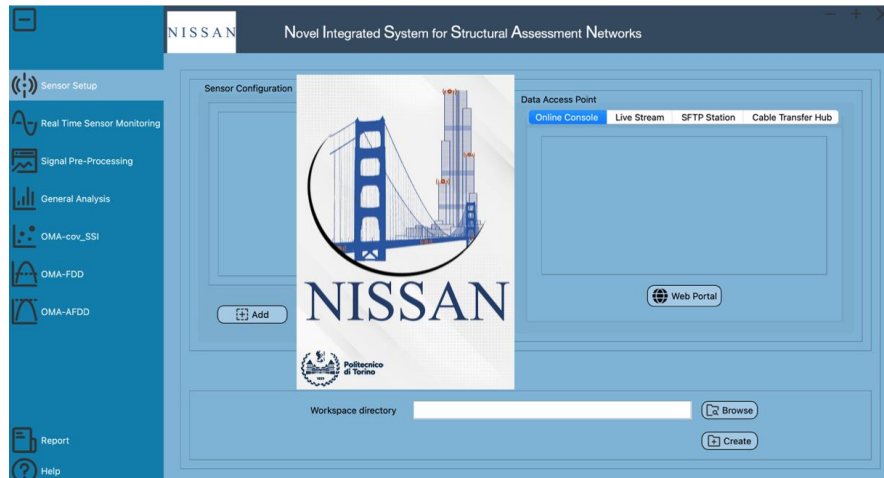


Fig. 5-1. A view of the developed software.

The interface is designed to perform a wide range of tasks, including:

- Data acquisition from instrumented sensors through a dedicated online console, live streaming via Wi-Fi, data streaming using the embedded FTP protocol, and cable transfer hub.
- Real-time monitoring of the data acquisition system, alongside plotting accelerations, velocities, and displacements in different domains.
- Preprocessing of acceleration records using Hanning window filtering, Butterworth filtering, and Singular Value Decomposition (SVD)-based algorithms. Coordinate system conversion is also included in this section.
- OMA analysis, including FDD, AFDD, SSI, and the extraction of modal properties from them.

The software is in its final stages of development and will be released soon by Lunitek. The collaborative effort with Lunitek has not only resulted in a convenient tool for OMA analysis but also represents a significant step towards making this technology more accessible and user-friendly for experts and newcomers.

## 6. CONCLUDING REMARKS

This study aimed to develop an automated FDD technique based on the MAC criterion to extract dynamic properties from ambient vibration responses. To incorporate a robust method, a comprehensive sensitivity analysis was conducted that assessed the impact of various factors, including MAC variation, noise levels, acceleration duration, and the number and placement of sensors. Stabilization diagrams were created by comparing AFDD results with the corresponding Finite Element (FE) counterparts using experimental data from the Yonghe cable-stayed. In the diagrams, unstable, sub-optimal, and optimal regions for MAC variation were defined based on the accuracy of estimated natural frequencies. Additionally, based on the analysis, the optimal range of hyperparameters present in the AFDD was derived, eliminating the need for further parameter tuning in each case study.

In the second part, the analysis involves three case studies with dissimilar mode shapes, structural systems, materials, and excitation sources. In each case study, the output-only modal identification was performed by employing traditional FDD, the optimized AFDD, and cov-SSI using field acceleration records. Based on the acquired properties, a direct comparison was made while evaluating their viability. In analyzing the Yonghe cable-stayed bridge, the AFDD had a superior performance in detecting accurate frequencies and tackling spurious modes with respect to cov-SSI. Conversely, the AFDD didn't identify a combined torsional mode despite accurately estimating frequencies for the PolyU footbridge. In the last case, the analysis of Massimo built heritage disclosed the better performance of AFDD in identifying torsional modes and weakly excited ones against cov-SSI. The following concluding remarks are made based on the outcomes:

- The AFDD optimal performance is observed with a MAC threshold of 0.2 when considering various factors influencing modal property estimations;

- AFDD outperforms cov-SSI in accurately estimating vertical and transversal modes, reducing ambiguity in interpreting stabilization diagrams, and minimizing user interference, while spurious mode identification is subsided;
- There is a high risk of not identifying torsional mode shapes where their geometry resembles the primary modes identified by AFDD, particularly with a low number of instrumented sensors. This limitation was observed in the second case study, where the torsional mode was not identified by AFDD but was estimated by cov-SSI;
- The previous study on the Molleta tower needs to be further extended by instrumenting new sensors in the system since a weakly excited mode of vibration was identified by AFDD analysis. Furthermore, the study observed a reduction in natural frequencies, indicating damage and stiffness loss.
- In the analysis of Moletta tower, the torsional movement of structure was captured in identified modes. Therefore, there is a need for further monitoring and in-depth studies to propose an intervention plan that prevent the twisting of the structure.

## 7. REFERENCES

- An, Y., E. Chatzi, S. Sim, S. Laflamme, B. Blachowski, and J. Ou. 2019. “Recent progress and future trends on damage identification methods for bridge structures.” *Struct. Control Health Monit.*, 26 (10). <https://doi.org/10.1002/stc.2416>.
- Bishop, C. M. 2009. *Pattern recognition and machine learning*. Information science and statistics. New York: Springer.
- Boroschek, R. L., and J. A. Bilbao. 2019. “Interpretation of stabilization diagrams using density-based clustering algorithm.” *Eng. Struct.*, 178: 245–257. <https://doi.org/10.1016/j.engstruct.2018.09.091>.
- Brincker, R. n.d. “Introduction to Operational Modal Analysis.” 375.
- Brincker, R., P. Andersen, and N.-J. Jacobsen. 2007. “Automated Frequency Domain Decomposition for Operational Modal Analysis.” *IMAC-XXIV Conf. Expo. Struct. Dyn.*
- Brincker, R., C. E. Ventura, and P. Andersen. n.d. “Damping Estimation by Frequency Domain Decomposition.” 7.
- Brincker, R., L. Zhang, and P. Andersen. 2001. “Modal identification of output-only systems using frequency domain decomposition.” *Smart Mater. Struct.*, 10 (3): 441–445. <https://doi.org/10.1088/0964-1726/10/3/303>.
- Cantieni, R. 2004. “Experimental methods used in system identification of civil engineering structures.”
- Dederichs, A. C., and O. Øiseth. 2023. “Experimental comparison of automatic operational modal analysis algorithms for application to long-span road bridges.” *Mech. Syst. Signal Process.*, 199: 110485. <https://doi.org/10.1016/j.ymsp.2023.110485>.
- Dempster, A. P., N. M. Laird, and D. B. Rubin. 1977. “Maximum Likelihood from Incomplete Data Via the EM Algorithm.” *J. R. Stat. Soc. Ser. B Methodol.*, 39 (1): 1–22. <https://doi.org/10.1111/j.2517-6161.1977.tb01600.x>.
- García-Macías, E., and F. Ubertini. 2021. “Structural assessment of bridges through ambient noise deconvolution interferometry: application to the lateral dynamic behaviour of a RC multi-span viaduct.” *Arch. Civ. Mech. Eng.*, 21 (3): 123. <https://doi.org/10.1007/s43452-021-00273-9>.
- Hermans, L., and H. Van Der Auweraer. 1999. “MODAL TESTING AND ANALYSIS OF STRUCTURES UNDER OPERATIONAL CONDITIONS: INDUSTRIAL APPLICATIONS.” *Mech. Syst. Signal Process.*, 13 (2): 193–216. <https://doi.org/10.1006/mssp.1998.1211>.
- Hill, M. D. n.d. “An experimental Verification of the Eigensystem Realization Algorithm for Vibration Parameter Identification.” 9.
- Jeong, S., H. Kim, J. Lee, and S.-H. Sim. 2021. “Automated wireless monitoring system for cable tension forces using deep learning.” *Struct. Health Monit.*, 20 (4): 1805–1821. <https://doi.org/10.1177/1475921720935837>.
- Kim, H., and S. Sim. 2019. “Automated peak picking using region-based convolutional neural network for operational modal analysis.” *Struct. Control Health Monit.*, 26 (11). <https://doi.org/10.1002/stc.2436>.

- Lee, S.-Y., T.-C. Huynh, and J.-T. Kim. 2018. "A practical scheme of vibration monitoring and modal analysis for caisson breakwater." *Coast. Eng.*, 137: 103–119. <https://doi.org/10.1016/j.coastaleng.2018.03.008>.
- Li, J., T. Bao, and C. E. Ventura. 2022. "A robust methodology for output-only modal identification of civil engineering structures." *Eng. Struct.*, 270: 114764. <https://doi.org/10.1016/j.engstruct.2022.114764>.
- Li, S., H. Li, Y. Liu, C. Lan, W. Zhou, and J. Ou. 2014. "SMC structural health monitoring benchmark problem using monitored data from an actual cable-stayed bridge: SMC STRUCTURAL HEALTH MONITORING BENCHMARK PROBLEM." *Struct. Control Health Monit.*, 21 (2): 156–172. <https://doi.org/10.1002/stc.1559>.
- Limongelli, M. P., and P. F. Giordano. 2020. "Vibration-based damage indicators: a comparison based on information entropy." *J. Civ. Struct. Health Monit.*, 10 (2): 251–266. <https://doi.org/10.1007/s13349-020-00381-9>.
- Magalhães, F., Á. Cunha, and E. Caetano. 2008a. "Dynamic monitoring of a long span arch bridge." *Eng. Struct.*, 30 (11): 3034–3044. <https://doi.org/10.1016/j.engstruct.2008.04.020>.
- Magalhães, F., Á. Cunha, and E. Caetano. 2008b. "Dynamic monitoring of a long span arch bridge." *Eng. Struct.*, 30 (11): 3034–3044. <https://doi.org/10.1016/j.engstruct.2008.04.020>.
- Magalhães, F., Á. Cunha, and E. Caetano. 2009. "Online automatic identification of the modal parameters of a long span arch bridge." *Mech. Syst. Signal Process.*, 23 (2): 316–329. <https://doi.org/10.1016/j.ymsp.2008.05.003>.
- "NExT.pdf." n.d.
- Pan, Y., M. Matilainen, S. Taskinen, and K. Nordhausen. 2022. "A review of second-order blind identification methods." *WIREs Comput. Stat.*, 14 (4). <https://doi.org/10.1002/wics.1550>.
- Papazafeiropoulos, G., and V. Plevris. 2018. "OpenSeismoMatlab: A new open-source software for strong ground motion data processing." *Heliyon*, 4 (9): e00784. <https://doi.org/10.1016/j.heliyon.2018.e00784>.
- Pereira, S., F. Magalhães, Á. Cunha, C. Moutinho, and J. Pacheco. 2021. "Modal identification of concrete dams under natural excitation." *J. Civ. Struct. Health Monit.*, 11 (2): 465–484. <https://doi.org/10.1007/s13349-020-00462-9>.
- Pereira, S., F. Magalhães, J. P. Gomes, and Á. Cunha. 2022. "Modal tracking under large environmental influence." *J. Civ. Struct. Health Monit.*, 12 (1): 179–190. <https://doi.org/10.1007/s13349-021-00536-2>.
- Puzzilli, L. M., G. Bongiovanni, P. Clemente, V. Di Fiore, and V. Verrubbi. 2021. "Effects of Anthropogenic and Ambient Vibrations on Archaeological Sites: The Case of the Circus Maximus in Rome." *Geosciences*, 11 (11): 463. <https://doi.org/10.3390/geosciences11110463>.
- Qu, C.-X., Y.-F. Liu, T.-H. Yi, and H.-N. Li. 2023. "Structural Damping Ratio Identification through Iterative Frequency Domain Decomposition." *J. Struct. Eng.*, 149 (5): 04023042. <https://doi.org/10.1061/JSENDH.STENG-11837>.
- Ravizza, G., R. Ferrari, E. Rizzi, and V. Dertimanis. 2021. "On the denoising of structural vibration response records from low-cost sensors: a critical comparison and assessment." *J. Civ. Struct. Health Monit.*, 11 (5): 1201–1224. <https://doi.org/10.1007/s13349-021-00502-y>.

- Sabamehr, A., C. Lim, and A. Bagchi. 2018. "System identification and model updating of highway bridges using ambient vibration tests." *J. Civ. Struct. Health Monit.*, 8 (5): 755–771. <https://doi.org/10.1007/s13349-018-0304-5>.
- Sanliturk, K. Y., and O. Cakar. 2005. "Noise elimination from measured frequency response functions." *Mech. Syst. Signal Process.*, 19 (3): 615–631. <https://doi.org/10.1016/j.ymsp.2004.04.005>.
- "SSI-VanOverschee-1996.pdf." n.d.
- Sunca, F., M. Ergün, A. C. Altunişik, M. Günaydin, and F. Y. Okur. 2021. "Modal identification and fatigue behavior of Eynel steel arch highway bridge with calibrated models." *J. Civ. Struct. Health Monit.*, 11 (5): 1337–1354. <https://doi.org/10.1007/s13349-021-00512-w>.
- Van Overschee, P., and B. De Moor. 1996. *Subspace Identification for Linear Systems*.
- Verboven, P. n.d. "A Poly-Reference Implementation of the Least-Squares Complex Frequency-Domain Estimator." 10.
- Vesterholm, K. K., R. Brincker, and A. Brandt. 2020. "Random decrement technique for detection and characterization of nonlinear behavior." *Mech. Syst. Signal Process.*, 143: 106841. <https://doi.org/10.1016/j.ymsp.2020.106841>.
- Wu, Wen-Hwa, Wang, Sheng-Wei, Chen, Chien-Chou, and Lai, Gwolong. 2016. "Mode identifiability of a cable-stayed bridge under different excitation conditions assessed with an improved algorithm based on stochastic subspace identification." *Smart Struct. Syst.*, 17 (3): 363–389. <https://doi.org/10.12989/SSS.2016.17.3.363>.
- Xia, Q., W. Wu, F. Li, Y. Xia, X. Ding, W. H. K. Lam, W. Chung, and Y. Xu. 2021. "System design and demonstration of performance monitoring of a butterfly-shaped arch footbridge." *Struct. Control Health Monit.*, 28 (7). <https://doi.org/10.1002/stc.2738>.
- Ye, X., P. Huang, C. Pan, and L. Mei. 2021. "Innovative stabilization diagram for automated structural modal identification based on ERA and hierarchical cluster analysis." *J. Civ. Struct. Health Monit.*, 11 (5): 1355–1373. <https://doi.org/10.1007/s13349-021-00514-8>.
- Zhong, Q.-M., S.-Z. Chen, Z. Sun, and L.-C. Tian. 2023. "Fully automatic operational modal analysis method based on statistical rule enhanced adaptive clustering method." *Eng. Struct.*, 274: 115216. <https://doi.org/10.1016/j.engstruct.2022.115216>.
- Zhou, K., Q.-S. Li, and X.-L. Han. 2022. "Modal Identification of Civil Structures via Stochastic Subspace Algorithm with Monte Carlo-Based Stabilization Diagram." *J. Struct. Eng.*, 148 (6): 04022066. [https://doi.org/10.1061/\(ASCE\)ST.1943-541X.0003353](https://doi.org/10.1061/(ASCE)ST.1943-541X.0003353).

God's praise be on Prophet, his Household, and his advocates.